Journal of Quantitative Spectroscopy & Radiative Transfer 316 (2024) 108921

Contents lists available at ScienceDirect

Journal of Quantitative Spectroscopy and Radiative Transfer

journal homepage: www.elsevier.com/locate/jqsrt

Determination of the radiative transition rates in Ta VII using a multiplatform approach

E. Bokamba Motoumba [a], S. Enzonga Yoca [a,b], P. Quinet [c,d], P. Palmeri [c,*]

[a] Faculté des Sciences et Techniques, Université Marien Ngouabi, Brazzaville, BP 69, Congo
[b] Conseil Africain et Malgache pour l'Enseignement Supérieur – CAMES, Ouagadougou 01, 01 BP 134, Burkina Faso
[c] Physique Atomique et Astrophysique, Université de Mons – UMONS, Mons, B 7000, Belgium
[d] IPNAS, Université de Liège, Liège, B 4000, Belgium

ARTICLE INFO

Keywords:
Atomic structure
Transition probabilities
Oscillator strengths
Ta VII spectrum

ABSTRACT

Tantalum ($Z = 73$) is an element that is produced in the neutron-induced transmutation of tungsten ($Z = 74$) which in turn will compose the divertors in Tokamaks. As a consequence, their sputtering may generate ionic impurities of all possible charge states in the deuterium-tritium plasma that could contribute to radiation losses in controlled nuclear devices. The radiative properties of these ions have therefore potential important applications in this field. In this context, a multiplatform approach has been adopted in order to compute the Ta VII radiative rates and estimate their accuracy. The oscillator strengths and transition probabilities have been calculated for the 237 electric dipole (E1) transitions of the Ta VII spectrum as classified by Ryabtev et al. (2014). Three independent atomic structure models have been used; one based on the semi-empirical pseudo-relativistic Hartree–Fock (HFR) method and two based on the fully relativistic *ab initio* multiconfiguration Dirac–Hartree–Fock (MCDHF) method.

1. Introduction

The main motivation of the present work is to provide the nuclear fusion community with the required atomic data. In that respect, future fusion devices such as ITER will use tungsten (W) as building material of its divertor, the part of the tokamak directly in contact with the most extreme fusion plasma conditions [1]. The neutrons produced by the deuterium-tritium fusion reactions will bombard the wall and the divertor. Tungsten present in the latter will transmute by neutron-capture mainly to rhenium (Re), osmium (Os) and tantalum (Ta) [2]. Moreover, tantalum by itself has been very recently studied as potential plasma-facing material in fusion reactors [3]. It could therefore diffuse into the fusion plasma as impurities in all its charge states and radiate, contributing to radiation losses in the energy balance of the nuclear reactor.

Few works have been published concerning the atomic structure and the radiative properties of Ta VII. Ryabtsev et al. [4] recorded using a grazing-incidence vacuum spectrograph a tantalum spectrum in the range 145–350 Å that was produced by a low-inductive vacuum spark. In that study, they have identified the $4f^{13}5s^25p^6 - 4f^{13}5s^25p^56s$ electric dipole (E1) transitions in Ta VII thanks to comparisons with their Hartree–Fock calculations. A few years later, the same group [5] extended the analysis of Ta VII by recording its spectrum in the region 300–500 Å using the 10 m normal incidence spectrograph in the Meudon Observatory. They classified 237 lines as E1 transitions from the excited even configurations $4f^{12}5s^25p^65d$, $4f^{12}5s^25p^66s$, $4f^{13}5s^25p^55d$, $4f^{13}5s^25p^56s$, $4f^{14}5s^25p^45d$, and $4f^{14}5s^25p^46s$ to the low-lying odd configurations $4f^{13}5s^25p^6$ and $4f^{14}5s^25p^5$. The Hartree–Fock calculation carried out by the authors helped for the line identification and the corresponding transition probabilities were published. However, their accuracy has not been evaluated.

In this paper, we present a multiplatform approach to determine the radiative rates in the spectrum of Ta^{6+}. It consists in using three independent atomic structure models in order to evaluate the transition probabilities along with their corresponding accuracies. In the following section, the computational methods and the models are described. In Section 3, the results are presented and discussed. The conclusions are given in Section 4.

2. Atomic structure and transition rate calculations

Three independent calculations have been carried out for the determination of the radiative parameters in Ta VII. Two were based on the purely *ab initio* MCDHF method [6] while a third one was based on the semi-empirical HFR method [7] that relies on the availability

* Corresponding author.
E-mail address: patrick.palmeri@umons.ac.be (P. Palmeri).

https://doi.org/10.1016/j.jqsrt.2024.108921
Received 14 November 2023; Received in revised form 23 January 2024; Accepted 23 January 2024
Available online 29 January 2024

of experimental energy levels. In what follows, we detail the three computations performed in this study.

2.1. Ab initio MCDHF-RCI method

The fully relativistic multiconfiguration Dirac–Hartree–Fock (MCDHF) method [6] was used as implemented in the GRASP2018 atomic structure computer package [8]. In this method [6], the atomic state function (ASF) $\Psi(\alpha \Pi J M_J)$ of parity Π, total angular momentum J, and its corresponding total magnetic quantum numbers M_J, is represented by a superposition of configuration state functions (CSF) $\Phi(\gamma \Pi J M_J)$, where γ and α respectively refer to a specific ASF and CSF.

The CSFs are constructed on jj-coupled N-electron Slater determinants of one-electron spin–orbitals, $\phi_{n\kappa m}(r,\theta,\varphi)$. Their corresponding large and small radial components are solutions of the radial integro-differential MCDHF equations and the relativistic quantum number κ is related to the non-relativistic orbital quantum number ℓ and the total quantum number j of the electron [6].

The CSFs in the expansions are generated from a set of configurations called multireference (MR) that includes the spectroscopic or targeted states and others that strongly interact with the latter. In these expansions, electrons from the occupied orbitals of the MR are excited to an active set of orbitals (AS). From now on, the AS will be denoted by a set of $n_{max}\ell$, where n_{max} will refer to the maximum principal quantum number of the orbital for a fixed value of the non-relativistic orbital quantum number ℓ of an excited electronic subshell.

2.1.1. MCDHF-RCI-A

Our first MCDHF-RCI model consisted in considering in the MR the following configurations: the ground configuration $4f^{13}$ and the first excited configuration $5p^5 4f^{14}$ both having an odd parity with symmetries $J^\Pi = 1/2^\circ - 7/2^\circ$; and the spectroscopic even-parity configurations $4f^{12}(5d+6s)$, $5p^5 4f^{13}(5d+6s)$, and $5p^4 4f^{14}(5d+6s)$ with symmetries $J^\Pi = 1/2^e - 9/2^e$. The AS was 6s6p6d6f. All the single and double electron excitations from occupied subshells except the core subshells up to the 4d subshell which were kept closed were performed in order to build a basis of 4 030 337 CSFs. The orbitals were obtained separately in single-configuration Dirac–Hartree–Fock Extended Average Level (EAL) [6,8] self-consistent-field (SCF) optimization where all the core orbitals, *i.e.* 1s to 4d, along with the 5s, 5p, and 4f valence orbitals were optimized on the ground configuration $5s^2 5p^6 4f^{13}$, and all the other orbitals $n\ell$ of the AS were optimized on a configuration of the corresponding type $5s^2 5p^6 4f^{12} n\ell$. Finally, further relativistic interactions have been included during the relativistic configuration interaction (RCI) procedure where the Dirac–Coulomb–Breit (DCB) Hamiltonian with the addition of the quantum electrodynamics (QED) terms such as the self-energy (SE) and the vacuum polarization (VP) interations has been diagonalized on the 4 030 337 CSFs basis to obtain the corresponding eigenvalues and eigenvectors.

2.1.2. MCDHF-RCI-B

For the second *ab initio* MCDHF-RCI model, a different strategy has been followed where the same MR as in our MCDHF-RCI-A model was adopted, but with an AS with one correlation shell per ℓ symmetry, namely 7s6p6d5f, along with a different optimization scheme. The latter was performed in three steps. The first step consisted in optimizing the core orbitals along with the 5s, 5p, and 4f orbitals on the ground configuration using an EAL procedure similarly as in our MCDHF-RCI-A model. In the second step, the remaining 5d and 6s valence orbitals were optimized during a MCDHF Extended Optimal Level (EOL) [6,8] SCF procedure on all the 255 levels of the MR keeping the orbitals of the preceding step frozen. Finally, in the last step, all the single and double excitations from the occupied 5s, 5p, 4f, 6s, and 6d orbitals to the AS were considered extending CSFs basis to 1 546 503 CSFs. The 7s, 6p, 6d, and 5f correlation orbitals were then optimized on the 255 levels of the MR using a MCDHF EOL procedure. The eigenvalues and eigenvectors were finally determined during an RCI calculation where the DCB Hamiltonian with the addition of the QED terms was build on the 1 546 503 CSFs basis and diagonalized.

2.2. Semi-empirical HFR method

An additional independent approach considered in this study was the Hartree–Fock with relativistic corrections (HFR) method of R. D. Cowan [7]. The atomic state functions were also superpositions of configuration state functions. Here, the CSFs were LSJ-coupled Slater determinants built from non-relativistic one-electron orbitals, $\phi_{nlm_lm_s}(r,\theta,\varphi,s_z)$, where s_z is the projection of the electron spin on the z-axis [7].

The radial orbitals were in turn solutions of the monoconfigurational HFR radial equations obtained by the variational principle on the configuration average energy E_{av} of each non-relativistic configuration considered in the model and where the relativistic mass-velocity and Darwin terms were added. The mixing coefficients of the expansions were then determined by solving in a second step the secular equation of the multiconfiguration Hamiltonian matrix where the spin–orbit operator was incorporated.

The following interacting configurations have been considered in the expansions of the ASFs: $4f^{13}$ + $5p^5 4f^{14}$ + $4f^{12}(6p+7p+5f+6f+7f)$ + $5p^4 4f^{14}(6p+7p+5f+6f+7f)$ + $5s5p^5 4f^{14}(5d+6s)$ in the odd parity; $4f^{12}(5d+6d+7d+6s+7s)$ + $5p^5 4f^{13}(5d+6d+7d+6s+7s)$ + $5s4f^{14}$ + $5s4f^{13}(6p+5f)$ + $5p^4 4f^{14}(5d+6d+7d+6s+7s)$ in even parity. The present expansion extends the configurations set of Ryabtsev et al. [5] in the odd parity with the inclusion of configurations $5p^4 4f^{14}(6p, 7p, 5f, 6f, 7f)$, $5s5p^5 4f^{14}(5d, 6s)$ and $4f^{12}(6p, 7p, 5f, 6f, 7f)$ and, in the even parity, of the configurations $5p^4 4f^{14}7d$, $5p^5 4f^{13}7d$ and $4f^{12}(7s, 7d)$.

In order to correct the mixing coefficients of the expansions to take into account missing highly excited interacting configurations, all the Slater integrals of the Hamiltonian have been scaled down by a factor 0.9 in a first step according to a well-established practice for highly-charged ions [7]. In a second step, a semi-empirical least-square fitting procedure has been carried out in which some radial parameters of the Hamiltonian, such as the configuration average energies, Slater and spin–orbit integrals, have been adjusted to minimize the differences between our Hamiltonian eigenvalues and the experimental level energies available in the literature [5]. The average deviation of the fitting procedures were 0 cm^{-1} for the odd parity with all known 4 levels of the $4f^{13}$ and $5p^5 4f^{14}$ configurations included and 315 cm^{-1} for even parity with all known 126 levels included, namely the levels belonging to the $4f^{12}(5d+6s)$, $5p^5 4f^{13}(5d+6s)$, and $5p^4 4f^{14}(5d+6s)$ configurations. Compared to the least-squared fit of Ryabtsev et al. [5] where they got a standard deviation of 380 cm^{-1} in the even parity, this is slightly higher as our average deviation for the even parity with 45 fitted parameters corresponds to a standard deviation of 393 cm^{-1} (see Eq. (16.1) of Ref. [7]). This may be explained by our choice to fix all the configuration-interaction parameters at 90% of their HFR values whereas Ryabtsev et al. [5] fixed them at 85% except for the $5p^5 4f^{13} - 4f^{12}6s$ and $5p^4 4f^{14} - 4f^{12}6s$ interactions where they were fitted. We report the radial parameters adopted for the calculation of the transition probabilities in Ta VII in Table 1.

3. Results and discussions

Table 2 presents our three sets of calculated energy levels, *i.e.* HFR, MCDHF-RCI-A and MCDHF-RCI-B, along with the values determined experimentally by Ryabtsev et al. [5]. As we focused on the transition probabilities, we do not show the many unobserved even-parity levels located between the experimentally established ones. In this table, we also report the LS-coupling compositions as determined in our HFR model with the first three major components. The latter shows that most of the levels are strongly mixed with a purity less or equal to 50%. In Figs. 1–3, the difference between our computed energy levels and the corresponding experimental values of Ryabtsev et al. [5] is plotted as function of the latter. The root mean squares (RMS) of these differences were 311 cm^{-1} for our HFR model (see Fig. 1), 12 073 cm^{-1} for our

Table 1
Radial parameters (in cm^{-1}) adopted in our HFR model for Ta VII.

Configuration	Parameter	*Ab Initio*	Fitted	Unc.	Ratio	Remark[a]
Odd parity						
$4f^{13}$	E_{av}	10 765	10 742	0	/	
	ζ_{4f}	4 448	4 393	0	0.99	
$5p^5 4f^{14}$	E_{av}	87 171	87 544	0	/	
	ζ_{5p}	51 311	51 308	0	1.00	
$5p^4 4f^{14} 6p$	E_{av}	621 604	/	/	/	F
$5p^4 4f^{14} 7p$	E_{av}	800 555	/	/	/	F
$5p^4 4f^{14} 5f$	E_{av}	721 323	/	/	/	F
$5p^4 4f^{14} 6f$	E_{av}	846 094	/	/	/	F
$5p^4 4f^{14} 7f$	E_{av}	912 444	/	/	/	F
$5s5p^5 4f^{14} 5d$	E_{av}	747 323	/	/	/	F
$5s5p^5 4f^{14} 6s$	E_{av}	850 322	/	/	/	F
$4f^{12} 6p$	E_{av}	521 395	/	/	/	F
$4f^{12} 7p$	E_{av}	705 642	/	/	/	F
$4f^{12} 5f$	E_{av}	624 284	/	/	/	F
$4f^{12} 6f$	E_{av}	751 739	/	/	/	F
$4f^{12} 7f$	E_{av}	819 411	/	/	/	F
Even parity						
$4f^{12} 5d$	E_{av}	338 299	338 317	182	/	
	$F^2(4f4f)$	168 562	138 149	1 771	0.82	
	$F^4(4f4f)$	107 001	88 886	5 214	0.83	
	$F^6(4f4f)$	77 344	69 036	2 648	0.89	
	ζ_{4f}	4 633	4 561	95	0.98	
	ζ_{5d}	4 150	4 052	136	0.98	
	$F^2(4f5d)$	42 628	35 519	/	0.83	f
	$F^4(4f5d)$	20 551	17 123	/	0.83	f
	$G^1(4f5d)$	15 041	13 726	/	0.91	f
	$G^3(4f5d)$	13 989	12 765	/	0.91	f
	$G^5(4f5d)$	11 154	10 180	/	0.91	f
$4f^{12} 6s$	E_{av}	452 398	452 013	485	/	
	$F^2(4f4f)$	169 011	140 266	3 000	0.83	
	$F^4(4f4f)$	107 311	82 185	10 828	0.77	
	$F^6(4f4f)$	77 575	73 184	7 286	0.94	
	ζ_{4f}	4 645	4 628	212	1.00	
	$G^3(4f6s)$	4 799	4 594	/	0.96	f
$5p^5 4f^{13} 5d$	E_{av}	369 037	368 977	189	/	
	ζ_{4f}	4 464	4 418	72	0.99	
	ζ_{5p}	53 889	53 429	161	0.99	
	ζ_{5d}	3 911	3 946	133	1.01	
	$F^2(4f5p)$	64 725	55 784	2 507	0.86	
	$F^2(4f5d)$	41 740	35 928	1 198	0.86	
	$F^4(4f5d)$	20 174	19 966	2 292	0.99	
	$F^2(5p5d)$	73 467	59 019	2 338	0.80	
	$G^2(4f5p)$	27 410	24 576	1 950	0.90	
	$G^4(4f5p)$	22 493	19 346	2 286	0.86	
	$G^1(4f5d)$	15 268	14 517	406	0.95	
	$G^3(4f5d)$	13 967	12 590	2 835	0.90	
	$G^5(4f5d)$	11 075	12 674	3 927	1.14	
	$G^1(5p5d)$	88 651	64 853	457	0.73	
	$G^3(5p5d)$	55 693	43 420	2 632	0.78	
$5p^5 4f^{13} 6s$	E_{av}	472 770	473 032	141	/	
	ζ_{4f}	4 475	4 349	66	0.97	
	ζ_{5p}	54 988	54 143	176	0.98	
	$F^2(4f5p)$	65 395	51 128	2 218	0.78	
	$G^2(4f5p)$	27 622	27 178	1 243	0.98	
	$G^4(4f5p)$	22 723	24 950	2 279	1.10	
	$G^1(4f6s)$	9 885	7 516	924	0.76	
	$G^3(4f6s)$	4 867	4 332	1 748	0.89	
$5p^4 4f^{14} 5d$	E_{av}	440 080	440 154	136	/	
	$F^2(5p5p)$	88 451	77 350	2 207	0.87	
	ζ_{5p}	52 019	51 738	210	0.99	
	ζ_{5d}	3 683	3 784	184	1.03	
	$F^2(5p5d)$	72 051	63 470	1 670	0.88	
	$G^1(5p5d)$	86 640	62 485	544	0.72	
	$G^3(5p5d)$	54 417	41 089	2 249	0.76	
$5p^4 4f^{14} 6s$	E_{av}	535 838	535 649	190	/	
	$F^2(5p5p)$	89 099	72 749	1 333	0.81	
	ζ_{5p}	53 083	52 990	199	1.00	
	$G^1(5p6s)$	9 903	9 592	919	0.97	
$4f^{12} 6d$	E_{av}	657 372	/	/	/	F
$4f^{12} 7d$	E_{av}	760 610	/	/	/	F
$4f^{12} 7s$	E_{av}	667 074	/	/	/	F
$5p^5 4f^{13} 6d$	E_{av}	676 413	/	/	/	F
$5p^5 4f^{13} 7d$	E_{av}	786 655	/	/	/	F
$5p^5 4f^{13} 7s$	E_{av}	702 059	/	/	/	F
$5s 4f^{14}$	E_{av}	407 975	/	/	/	F
$5s\ 4f^{13} 6p$	E_{av}	943 952	/	/	/	F
$5s\ 4f^{13} 5f$	E_{av}	1 043 769	/	/	/	F
$5p^4 4f^{14} 6d$	E_{av}	736 029	/	/	/	F
$5p^4 4f^{14} 7d$	E_{av}	854 790	/	/	/	F
$5p^4 4f^{14} 7s$	E_{av}	761 648	/	/	/	F

(*continued on next page*)

Table 1 (*continued*).

[a] F: fixed; f: fixed to the value taken from Ryabtsev et al. [5].

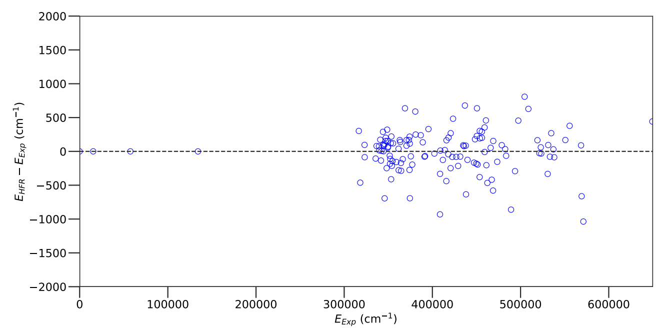

Fig. 1. Comparison of HFR energy levels with respect to experiment [5]. The energy difference is plotted versus the experimental energy. The root mean square of the differences is equal to 311 cm^{-1}. Black dashed line: straight line of equality.

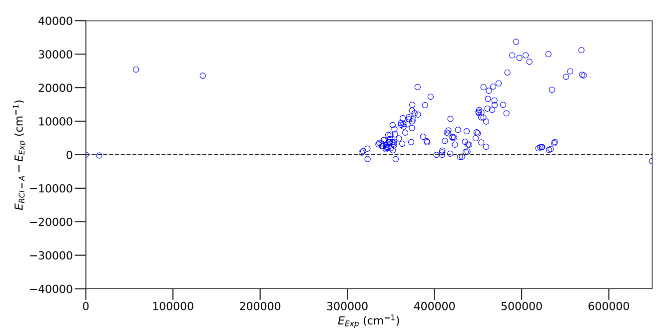

Fig. 2. Comparison of MCDHF-RCI-A energy levels with respect to experiment [5]. The energy difference is plotted versus the experimental energy. The root mean square of the differences is equal to 12 073 cm^{-1}. Black dashed line: straight line of equality.

MCDHF-RCI-A model (see Fig. 2), and 9580 cm^{-1} for our MCDHF-RCI-B model (see Fig. 3). As our semi-empirical HFR model was fitted to minimize the differences between the calculated and experimental energy levels, it is therefore not surprising that it reproduces better the experimental energy spectrum as it can been seen in Fig. 1. Concerning our *ab initio* structure models, our MCDHF-RCI-B energy levels agree much better with experiment than our MCDHF-RCI-A calculation. Indeed, our MCDHF-RCI-B representation of the correlation effects seems better than in our MCDHF-RCI-A model, probably because of a better choice of orbitals, meaning the inclusion of correlation orbitals correcting the targeted or spectroscopic ones.

In Table 3, we report the weighted transition probabilities or Einstein coefficients for spontaneous emission process, gA, the weighted oscillator strengths in the logarithmic scale, $log\ gf$, with their corresponding uncertainty indicators, *i.e.* the cancellation factor (CF) as defined by Cowan [7] for the HFR method and the uncertainty indicator dT as defined by Ekman et al. [9] for the MCDHF method, as computed in our three independent models for the 237 electric dipole transitions classified by Ryabtsev et al. [5] between 190 Å and 355 Å in Ta VII. In this table, our MCDHF-RCI-A/B transition rates have been rescaled

Table 2
Comparison between experimental, HFR, MCDHF-RCI-A and MCDHF-RCI-B energy levels in Ta VII.

i	E_{Exp} [a] (cm^{-1})	E_{HFR} [b] (cm^{-1})	E_{RCI-A} [c] (cm^{-1})	E_{RCI-B} [d] (cm^{-1})	J	LS-coupling composition [e]
1	0	0	0	0	7/2	99% $4f^{13}\ ^2F^o$
2	15 379.5	15 380	15 139	15 122	5/2	99% $4f^{13}\ ^2F^o$
3	57 512.8	57 513	82 929	72 950	3/2	99% $5p^54f^{13}\ (^1S)^2P^o$
4	134 169.4	134 169	157 743	148 352	1/2	99% $5p^54f^{13}\ (^1S)^2P^o$
5	316 576	316 878	317 213	312 788	7/2	62% $4f^{12}5d\ (^3H)^2F$ + 8% $4f^{12}5d\ (^3H)^4G$ + 6% $4f^{12}5d\ (^3F)^4G$
6	318 200	317 738	319 296	316 872	5/2	28% $4f^{12}5d\ (^3H)^4F$ + 13% $4f^{12}5d\ (^3F)^4F$ + 10% $4f^{12}5d\ (^1G)^2D$
7	323 083	323 179	324 885	324 500	7/2	43% $4f^{12}5d\ (^3F)^4G$ + 11% $4f^{12}5d\ (^3F)^4H$ + 11% $4f^{12}5d\ (^3H)^2F$
8	323 227	323 141	321 930	323 742	5/2	28% $4f^{12}5d\ (^3F)^4G$ + 18% $5p^54f^{13}5d\ (^3F)^4G$ + 13% $4f^{12}5d\ (^1D)^2F$
9	335 651	335 545	338 746	343 994	5/2	14% $4f^{12}5d\ (^3F)^2D$ + 12% $5p^54f^{13}5d\ (^3D)^4G$ + 11% $5p^54f^{13}5d\ (^1D)^2F$
10	336 678	336 757	340 228	336 317	5/2	22% $4f^{12}5d\ (^3F)^2F$ + 11% $4f^{12}5d\ (^3H)^2F$ + 10% $4f^{12}5d\ (^3F)^4D$
11	339 423	339 498	342 770	339 923	9/2	17% $4f^{12}5d\ (^3F)^2H$ + 12% $4f^{12}5d\ (^1G)^2G$ + 11% $4f^{12}5d\ (^3H)^2H$
12	339 824	339 839	342 330	338 095	5/2	16% $5p^54f^{13}5d\ (^1D)^2F$ + 11% $4f^{12}5d\ (^3F)^4G$ + 9% $5p^54f^{13}5d\ (^3D)^4F$
13	340 890	341 062	343 492	341 520	5/2	23% $4f^{12}5d\ (^3H)^2F$ + 13% $4f^{12}5d\ (^1G)^2D$ + 8% $4f^{12}5d\ (^3H)^4G$
14	341 724	341 589	346 004	360 418	5/2	10% $4f^{12}5d\ (^3P)^4D$ + 9% $5p^54f5d\ (^3D)^4G$ + 9% $4f^{12}5d\ (^3P)^2D$
15	342 476	342 484	346 912	346 063	9/2	20% $4f^{12}5d\ (^1I)^2G$ + 13% $4f^{12}5d\ (^3H)^2H$ + 12% $4f^{12}5d\ (^3F)^2H$
16	343 986	344 275	346 786	344 356	5/2	18% $5p^54f^{13}5d\ (^3F)^4D$ + 18% $5p^54f^{13}5d\ (^3F)^4F$ + 10% $5p^54f^{13}5d\ (^1D)^2D$
17	344 131	344 229	345 752	345 160	7/2	14% $5p^54f^{13}5d\ (^3G)^4G$ + 10% $5p^54f^{13}5d\ (^3F)^4G$ + 8% $5p^54f^{13}5d\ (^1G)^2F$
18	344 538	344 540	346 641	344 594	7/2	11% $5p^54f^{13}5d\ (^3G)^2F$ + 10% $5p^54f^{13}5d\ (^1G)^2F$ + 9% $5p^54f^{13}5d\ (^3F)^4H$
19	344 949	345 033	347 869	343 260	9/2	23% $5p^54f^{13}5d\ (^1F)^2G$ + 15% $5p^54f^{13}5d\ (^3F)^4G$ + 9% $5p^54f^{13}5d\ (^3F)^4F$
20	345 842	345 148	348 200	330 520	5/2	12% $4f^{12}5d\ (^3F)^2F$ + 11% $4f^{12}5d\ (^1G)^2F$ + 8% $5p^54f^{13}5d\ (^3G)^2D$
21	345 929	346 037	347 948	347 726	3/2	12% $5p^54f^{13}5d\ (^3D)^2D$ + 11% $5p^54f^{13}5d\ (^1D)^2P$ + 11% $4f^{12}5d\ (^1G)^2D$
22	346 965	347 119	352 861	348 365	5/2	10% $5p^54f^{13}5d\ (^3D)^4G$ + 9% $5p^54f^{13}5d\ (^3D)^4D$ + 9% $5p^54f^{13}5d\ (^3D)^4F$
23	347 073	347 274	350 783	349 995	7/2	15% $5p^54f^{13}5d\ (^1D)^2F$ + 11% $4f^{12}5d\ (^3P)^2F$ + 7% $4f^{12}5d\ (^1D)^2G$
24	348 128	347 880	351 759	334 005	3/2	22% $4f^{12}5d\ (^1G)^2D$ + 13% $5p^54f^{13}5d\ (^3D)^4F$ + 9% $4f^{12}5d\ (^3H)^4F$
25	348 726	349 047	352 477	349 433	7/2	8% $4f^{12}5d\ (^1D)^2G$ + 8% $5p^54f^{13}5d\ (^3D)^4F$ + 7% $5p^54f^{13}5d\ (^1G)^2F$
26	349 140	349 294	353 801	352 303	7/2	10% $5p^54f^{13}5d\ (^1D)^2F$ + 8% $4f^{12}5d\ (^3P)^4D$ + 7% $5p^54f^{13}5d\ (^3D)^2G$
27	349 511	349 568	355 504	348 975	3/2	24% $5p^54f^{13}5d\ (^3F)^2P$ + 17% $5p^54f^{13}5d\ (^3D)^2P$ + 13% $5p^54f^{13}5d\ (^3F)^2D$
28	349 833	349 904	351 780	350 768	5/2	11% $4f^{12}5d\ (^1G)^2F$ + 9% $4f^{12}5d\ (^3H)^4G$ + 8% $4f^{12}5d\ (^3F)^2D$
29	351 668	351 604	355 449	352 202	9/2	13% $5p^54f^{13}5d\ (^1G)^2G$ + 13% $5p^54f^{13}5d\ (^3F)^2G$ + 12% $5p^54f^{13}5d\ (^3D)^4F$
30	351 959	351 776	360 787	353 960	3/2	31% $5p^54f^{13}5d\ (^3D)^4F$ + 9% $5p^54f^{13}5d\ (^3D)^4D$ + 8% $5p^54f^{13}5d\ (^3D)^2D$
31	352 246	352 135	353 573	355 639	5/2	12% $5p^54f^{13}5d\ (^1D)^2D$ + 9% $5p^54f^{13}5d\ (^3D)^4D$ + 8% $5p^54f^{13}5d\ (^3D)^2F$
32	352 887	353 009	356 181	357 857	5/2	15% $4f^{12}5d\ (^3P)^2D$ + 14% $5p^54f^{13}5d\ (^1G)^2F$ + 7% $5p^54f^{13}5d\ (^3D)^4F$
33	353 224	352 812	357 031	354 688	7/2	28% $4f^{12}5d\ (^1I)^2G$ + 14% $5p^54f^{13}5d\ (^3D)^2G$ + 9% $5p^54f^{13}5d\ (^3G)^4F$
34	353 523	353 743	356 314	353 548	9/2	18% $5p^54f^{13}5d\ (^3G)^4H$ + 18% $5p^54f^{13}5d\ (^1G)^2H$ + 8% $5p^54f^{13}5d\ (^3D)^4G$
35	354 068	353 855	361 647	357 003	7/2	29% $4f^{12}5d\ (^3P)^4D$ + 9% $4f^{12}5d\ (^3P)^2F$ + 8% $4f^{12}5d\ (^3H)^4H$
36	354 746	354 602	360 826	364 743	5/2	13% $5p^54f^{13}5d\ (^3D)^2F$ + 13% $4f^{12}5d\ (^3P)^2D$ + 9% $5p^54f^{13}5d\ (^3G)\ 4F$
37	355 450	355 569	354 126	361 732	3/2	29% $4f^{12}5d\ (^3P)^4F$ + 23% $4f^{12}5d\ (^1D)^2D$ + 21% $4f^{12}5d\ (^3P)^4D$
38	359 169	359 012	364 024	361 821	7/2	33% $4f^{12}5d\ (^1I)^2G$ + 12% $5p^54f^{13}5d\ (^1G)^2G$ + 10% $5p^54f^{13}5d\ (^3G)^2G$
39	361 634	361 673	371 075	365 872	5/2	20% $5p^54f^{13}5d\ (^3D)^2F$ + 17% $5p^44f^{14}5d\ (^3P)^4D$ + 10% $5p^54f^{13}5d\ (^3D)^4D$
40	361 737	361 459	370 650	365 844	3/2	30% $4f^{12}5d\ (^3P)^4F$ + 10% $5p^54f^{13}5d\ (^3D)^4F$ + 8% $5p^54f^{13}5d\ (^3D)^4D$
41	363 030	363 197	366 298	367 925	7/2	13% $4f^{12}5d\ (^1D)^2F$ + 10% $4f^{12}5d\ (^3P)^4F$ + 8% $5p^54f^{13}5d\ (^3F)^2G$
42	363 604	363 743	374 494	369 633	3/2	35% $4f^{12}5d\ (^3P)^4P$ + 21% $4f^{12}5d\ (^3P)^2P$ + 8% $4f^{12}5d\ (^3P)^2D$
43	364 365	364 194	373 514	369 116	5/2	17% $4f^{12}5d\ (^1D)^2D$ + 16% $4f^{12}5d\ (^3P)^4F$ + 14% $4f^{12}5d\ (^3P)^4P$
44	364 584	364 297	372 995	365 928	7/2	13% $4f^{12}5d\ (^1D)^2F$ + 10% $5p^54f^{13}5d\ (^3F)^2G$ + 10% $4f^{12}5d\ (^3P)^4D$
45	366 449	366 334	373 036	369 220	9/2	24% $4f^{12}5d\ (^1I)^2H$ + 15% $5p^54f^{13}5d\ (^3G)^2H$ + 12% $5p^54f^{13}5d\ (^1G)^2G$
46	368 941	369 578	378 009	380 058	5/2	30% $5p^44f^{14}5d\ (^3P)^4D$ + 13% $5p^54f^{13}5d\ (^3D)^4F$ + 9% $4f^{12}5d\ (^3P)^2D$
47	370 659	370 743	381 856	376 916	5/2	28% $4f^{12}5d\ (^3P)^2F$ + 14% $4f^{12}5d\ (^3P)^2D$ + 13% $4f^{12}5d\ (^1D)^2D$
48	370 725	370 893	381 301	371 333	7/2	41% $4f^{12}5d\ (^3P)^2F$ + 15% $4f^{12}5d\ (^1D)^2F$ + 11% $4f^{12}5d\ (^3P)^4F$
49	373 325	373 493	377 086	377 535	9/2	19% $5p^54f^{13}5d\ (^3D)^4G$ + 18% $5p^54f^{13}5d\ (^1G)^2H$ + 9% $4f^{12}5d\ (^1I)^2G$
50	374 091	373 817	382 050	396 765	7/2	26% $5p^44f^{13}5d\ (^3P)^4D$ + 21% $5p^44f^{13}5d\ (^3P)^4F$ + 11% $4f^{12}5d\ (^3P)^4F$
51	374 198	374 416	387 331	396 070	5/2	13% $4f^{12}5d\ (^3P)^2D$ + 11% $5p^54f^{13}5d\ (^3G)^4D$ + 9% $5p^54f^{13}5d\ (^3F)^4P$
52	374 387	374 502	384 351	378 781	9/2	44% $4f^{12}5d\ (^1D)^2G$ + 39% $4f^{12}5d\ (^3P)^4F$ + 4% $4f^{12}5d\ (^3F)^2H$
53	374 516	373 823	389 393	383 018	1/2	24% $5p^44f^{14}5d\ (^3P)^4D$ + 23% $5p^44f^{14}5d\ (^3P)^2P$ + 23% $5p^44f^{14}5d\ (^1D)^2P$
54	375 580	375 507	386 143	380 330	3/2	29% $4f^{12}5d\ (^3P)^4P$ + 28% $4f^{12}5d\ (^3P)^2P$ + 28% $4f^{12}5d\ (^1D)^2P$
55	377 185	376 990	389 561	382 168	7/2	16% $5p^54f^{13}5d\ (^3D)^4F$ + 8% $5p^54f^{13}5d\ (^3G)^4G$ + 8% $5p^54f^{13}5d\ (^1D)^2F$
56	380 623	381 212	400 821	392 089	9/2	63% $5p^44f^{14}5d\ (^3P)^4F$ + 21% $5p^44f^{14}5d\ (^1D)^2G$ + 5% $4f^{12}5d\ (^3P)^4F$
57	381 044	381 293	393 022	383 475	7/2	35% $5p^44f^{14}5d\ (^3P)^2F$ + 16% $5p^44f^{14}5d\ (^1D)^2G$ + 15% $5p^44f^{14}5d\ (^3P)^4D$
58	386 824	387 063	392 194	402 731	3/2	11% $5p^44f^{14}5d\ (^3P)^4P$ + 11% $5p^44f^{14}5d\ (^1S)^2D$ + 9% $5p^54f^{13}5d\ (^3G)^4F$
59	389 091	389 225	403 888	390 127	7/2	20% $5p^54f^{13}5d\ (^3G)^4H$ + 11% $5p^54f^{13}5d\ (^1G)^2G$ + 10% $5p^54f^{13}5d\ (^3D)^2G$
60	391 106	391 028	395 120	391 490	3/2	20% $5p^44f^{14}5d\ (^1S)^2D$ + 10% $5p^54f^{13}5d\ (^3G)^4D$ + 10% $5p^54f^{13}5d\ (^3G)^4F$
61	391 745	391 675	395 461	374 906	5/2	29% $5p^54f^{13}5d\ (^3G)^4G$ + 8% $5p^54f^{13}5d\ (^1G)^2F$ + 7% $5p^54f^{13}5d\ (^3F)^2F$
62	395 564	395 894	412 877	396 034	3/2	26% $5p^54f^{13}5d\ (^3D)^4P$ + 24% $5p^54f^{13}5d\ (^3D)^4S$ + 15% $5p^54f^{13}5d\ (^1F)^2P$
63	402 297	402 265	402 230	403 550	5/2	23% $5p^54f^{13}5d\ (^3D)^4D$ + 17% $5p^54f^{13}5d\ (^3D)^4P$ + 8% $5p^54f^{13}5d\ (^1G)^2D$
64	408 640	407 709	409 336	384 046	1/2	40% $5p^44f^{14}5d\ (^3P)^4P$ + 10% $5p^54f^{13}5d\ (^3F)^4P$ + 9% $5p^44f^{14}5d\ (^3P)^2P$
65	408 707	408 375	408 685	410 261	9/2	18% $5p^54f^{13}5d\ (^1G)^2H$ + 15% $5p^54f^{13}5d\ (^3G)^4I$ + 12% $5p^54f^{13}5d\ (^3D)^2G$
66	409 045	409 057	410 272	421 655	3/2	31% $4f^{12}5d\ (^1S)^2D$ + 16% $5p^44f^{14}5d\ (^3P)^4P$ + 11% $5p^44f^{14}5d\ (^3P)^2D$
67	411 905	411 779	416 034	413 408	3/2	26% $5p^54f^{13}5d\ (^1G)^2D$ + 19% $5p^54f^{13}5d\ (^3G)^4D$ + 16% $5p^54f^{13}5d\ (^3F)^2P$
68	414 137	414 156	420 731	417 694	5/2	15% $5p^44f^{14}5d\ (^1D)^2F$ + 13% $5p^44f^{14}5d\ (^3P)^4F$ + 7% $5p^54f^{13}5d\ (^1G)^2F$
69	415 827	415 388	422 187	415 988	5/2	25% $5p^54f^{13}5d\ (^1G)^2F$ + 17% $5p^54f^{13}5d\ (^3G)^2F$ + 10% $5p^54f^{13}5d\ (^3F)^2D$
70	415 991	416 155	423 226	417 241	3/2	29% $5p^54f^{13}5d\ (^3D)^2P$ + 11% $5p^54f^{13}5d\ (^3D)^2D$ + 10% $5p^54f^{13}5d\ (^3D)^4D$
71	418 077	418 035	418 384	419 759	7/2	19% $5p^54f^{13}5d\ (^3D)^4D$ + 15% $5p^54f^{13}5d\ (^3D)^2F$ + 11% $5p^54f^{13}5d\ (^3F)^4D$

(*continued on next page*)

Table 2 (*continued*).

i	E_{Exp} [a] (cm^{-1})	E_{HFR} [b] (cm^{-1})	E_{RCI-A} [c] (cm^{-1})	E_{RCI-B} [d] (cm^{-1})	J	LS-coupling composition [e]
72	418 334	418 538	429 038	431 145	3/2	33% $4f^{12}5d\ (^{1}S)^{2}D$ + 18% $5p^{4}4f^{14}5d\ (^{3}P)^{4}F$ + 8% $5p^{4}4f^{14}5d\ (^{1}S)^{2}D$
73	420 660	420 412	425 769	422 113	5/2	19% $5p^{5}4f^{13}5d\ (^{3}D)^{2}D$ + 18% $5p^{5}4f^{13}5d\ (^{3}D)^{4}P$ + 8% $5p^{5}4f^{13}5d\ (^{3}F)^{4}G$
74	420 776	421 045	426 068	410 661	1/2	23% $5p^{5}4f^{13}5d\ (^{1}F)^{2}P$ + 20% $5p^{5}4f^{13}5d\ (^{3}G)^{4}D$ + 12% $5p^{5}4f^{13}5d\ (^{3}D)^{4}P$
75	422 564	422 482	427 692	423 054	5/2	18% $5p^{5}4f^{13}5d\ (^{3}D)^{2}D$ + 13% $4f^{12}5d\ (^{1}S)^{2}D$ + 11% $5p^{5}4f^{13}5d\ (^{1}D)^{2}F$
76	423 447	423 930	426 461	424 480	3/2	15% $5p^{5}4f^{13}5d\ (^{3}G)^{4}F$ + 15% $5p^{5}4f^{13}5d\ (^{3}D)^{2}P$ + 13% $5p^{5}4f^{13}5d\ (^{1}D)^{2}D$
77	426 995	426 914	434 417	436 587	5/2	50% $4f^{12}5d\ (^{1}S)^{2}D$ + 17% $5p^{4}4f^{14}5d\ (^{3}P)^{4}F$ + 7% $5p^{4}4f^{14}5d\ (^{1}S)^{2}D$
78	429 186	428 971	428 580	430 022	9/2	21% $5p^{5}4f^{13}5d\ (^{1}D)^{2}G$ + 19% $5p5^{4}f^{13}5d\ (^{3}G)^{2}H$ + 15% $5p^{5}4f^{13}5d\ (^{3}G)^{4}H$
79	431 589	431 512	431 001	432 385	7/2	25% $5p^{5}4f^{13}5d\ (^{3}G)^{4}G$ + 24% $5p^{5}4f^{13}5d\ (^{3}G)^{4}H$ + 15% $5p^{5}4f^{13}5d\ (^{3}G)^{2}G$
80	434 962	435 052	438 820	433 650	7/2	39% $5p^{5}4f^{13}6s\ (^{1}F)^{2}F$ + 24% $5p^{5}4f^{13}6s\ (^{3}D)^{4}D$ + 21% $5p^{5}4f^{13}6s\ (^{3}F)^{4}F$
81	435 796	435 874	436 608	434 606	5/2	55% $5p^{5}4f^{13}6s\ (^{1}F)^{2}F$ + 19% $5p^{5}4f^{13}6s\ (^{3}D)^{2}D$ + 10% $5p^{5}4f^{13}6s\ (^{3}D)^{4}D$
82	436 908	437 586	443 904	441 083	5/2	27% $5p^{5}4f^{13}5d\ (^{1}D)^{2}D$ + 11% $5p^{5}4f^{13}5d\ (^{3}D)^{2}F$ + 10% $5p^{5}4f^{13}5d\ (^{3}F)^{4}F$
83	437 867	437 952	438 820	437 400	7/2	47% $5p^{5}4f^{13}6s\ (^{3}F)^{2}F$ + 14% $5p^{5}4f^{13}6s\ (^{1}F)^{2}F$ + 9% $5p^{5}4f^{13}6s\ (^{3}G)^{4}G$
84	438 147	437 512	441 166	440 502	7/2	23% $5p^{5}4f^{13}5d\ (^{1}D)^{2}F$ + 16% $5p^{5}4f^{13}5d\ (^{3}F)^{2}G$ + 7% $5p^{5}4f^{13}5d\ (^{3}D)^{4}F$
85	439 812	439 687	442 809	441 226	9/2	73% $5p^{5}4f^{13}6s\ (^{3}G)^{2}G$ + 23% $5p^{5}4f^{13}6s\ (^{3}G)^{4}G$ + 4% $5p^{5}4f^{13}6s\ (^{3}F)^{4}F$
86	447 204	447 038	452 112	446 675	7/2	19% $5p^{5}4f^{13}6s\ (^{3}F)^{4}F$ + 19% $4f^{12}6s\ (^{3}F)^{2}F$ + 17% $4f^{12}6s\ (^{3}F)^{4}F$
87	448 343	448 522	455 048	447 267	5/2	49% $4f^{12}6s\ (^{3}F)^{2}F$ + 14% $4f^{12}6s\ (^{1}D)^{2}D$ + 14% $5p^{5}4f^{13}6s\ (^{3}F)^{4}F$
88	449 786	449 605	456 152	449 756	5/2	31% $5p^{5}4f^{13}6s\ (^{3}F)^{4}F$ + 27% $4f^{12}6s\ (^{3}F)^{2}F$ + 14% $4f^{12}6s\ (^{3}F)^{4}F$
89	450 406	450 634	463 254	465 527	9/2	31% $5p^{5}4f^{13}5d\ (^{3}D)^{2}G$ + 19% $5p^{5}4f^{13}5d\ (^{3}F)^{2}G$ + 11% $5p^{5}4f^{13}5d\ (^{3}G)^{2}G$
90	450 596	451 233	463 085	460 688	7/2	36% $5p^{4}4f^{14}5d\ (^{3}P)^{4}F$ + 16% $5p^{4}4f^{14}5d\ (^{3}P)^{4}D$ + 8% $5p^{4}4f^{14}5d\ (^{3}P)^{2}F$
91	451 282	451 088	464 625	466 096	5/2	28% $5p^{5}4f^{13}5d\ (^{3}G)^{2}D$ + 16% $5p^{5}4f^{13}5d\ (^{1}G)^{2}D$ + 12% $5p^{5}4f^{13}5d\ (^{3}F)^{2}D$
92	453 600	453 220	464 734	452 571	3/2	50% $5p^{5}4f^{13}6s\ (^{3}F)^{4}F$ + 36% $5p^{5}4f^{13}6s\ (^{3}D)^{4}D$ + 9% $5p^{5}4f^{13}6s\ (^{3}D)^{2}D$
93	453 747	454 050	457 413	454 610	5/2	41% $5p^{5}4f^{13}6s\ (^{3}F)^{2}F$ + 21% $5p^{5}4f^{13}6s\ (^{3}D)^{4}D$ + 12% $5p^{5}4f^{13}6s\ (^{3}D)^{2}D$
94	453 859	454 052	466 474	469 055	7/2	18% $5p^{5}4f^{13}5d\ (^{3}G)^{2}F$ + 14% $5p^{5}4f^{13}5d\ (^{3}F)^{2}F$ + 12% $5p^{5}4f^{13}5d\ (^{1}G)^{2}F$
95	456 112	456 403	467 192	470 694	7/2	32% $5p^{4}4f^{14}5d\ (^{1}D)^{2}G$ + 17% $5p^{4}4f^{14}5d\ (^{3}P)^{2}F$ + 6% $5p^{5}4f^{13}5d\ (^{3}G)^{2}G$
96	456 232	456 433	476 365	469 506	5/2	24% $5p^{4}4f^{13}5d\ (^{3}P)^{4}F$ + 18% $5p^{4}4f^{14}5d\ (^{1}D)^{2}F$ + 15% $5p^{4}4f^{14}5d\ (^{3}P)^{2}D$
97	459 200	459 554	461 581	470 161	3/2	22% $5p^{4}4f^{14}5d\ (^{3}P)^{2}P$ + 20% $5p^{4}4f^{14}5d\ (^{1}D)^{2}P$ + 16% $5p^{4}4f^{14}5d\ (^{3}P)^{4}P$
98	459 248	459 239	469 147	459 354	7/2	42% $4f^{12}6s\ (^{3}H)^{4}H$ + 40% $4f^{12}6s\ (^{1}G)^{2}G$ + 7% $4f^{12}6s\ (^{3}F)^{2}F$
99	460 725	461 183	474 481	461 511	7/2	39% $5p^{5}4f^{13}6s\ (^{1}G)^{2}G$ + 27% $5p^{5}4f^{13}6s\ (^{3}G)^{4}G$ + 20% $5p^{5}4f^{13}6s\ (^{3}G)^{2}G$
100	461 247	461 043	477 916	462 764	3/2	51% $5p^{5}4f^{13}6s\ (^{3}D)^{2}D$ + 26% $5p^{5}4f^{13}6s\ (^{3}D)^{4}D$ + 5% $5p^{4}4f^{13}5d\ (^{1}D)^{2}P$
101	462 366	461 900	481 457	473 874	5/2	51% $5p^{4}4f^{14}5d\ (^{3}P)^{2}F$ + 29% $5p^{4}4f^{13}5d\ (^{3}P)^{4}P$ + 6% $5p^{4}4f^{13}5d\ (^{1}D)^{2}F$
102	466 063	466 116	479 463	481 360	3/2	41% $5p^{5}4f^{13}5d\ (^{3}G)^{2}D$ + 6% $5p^{5}4f^{13}5d\ (^{3}F)^{2}D$ + 6% $5p^{5}4f^{13}5d\ (^{1}F)^{2}D$
103	467 320	466 901	487 656	479 886	9/2	66% $5p^{4}4f^{14}5d\ (^{1}D)^{2}G$ + 20% $5p^{4}4f^{14}5d\ (^{3}P)^{4}F$ + 5% $5p^{5}4f^{13}5d\ (^{1}D)^{2}G$
104	468 815	468 236	485 008	483 618	7/2	19% $5p^{5}4f^{13}5d\ (^{1}D)^{2}G$ + 13% $5p^{4}4f^{14}5d\ (^{1}D)^{2}G$ + 13 $5p^{5}4f^{13}5d\ (^{3}F)^{2}G$
105	469 039	469 193	483 844	484 068	5/2	27% $5p^{5}4f^{13}5d\ (^{3}G)^{2}F$ + 15% $5p^{5}4f^{13}5d\ (^{3}F)^{2}F$ + 11% $5p^{5}4f^{13}5d\ (^{1}D)^{2}F$
106	473 550	473 396	494 832	486 546	5/2	36% $5p^{4}4f^{14}5d\ (^{1}D)^{2}D$ + 22% $5p^{4}4f^{14}5d\ (^{1}D)^{2}F$ + 14% $5p^{4}4f^{14}6s\ (^{3}P)^{4}P$
107	478 697	478 789	493 573	489 999	5/2	55% $5p^{4}4f^{14}6s\ (^{3}P)^{4}P$ + 14% $5p^{4}4f^{14}6s\ (^{1}D)^{2}D$ + 10% $5p^{4}4f^{14}5d\ (^{1}D)^{2}D$
108	482 583	482 616	494 928	494 197	3/2	33% $5p^{4}4f^{14}6s\ (^{3}P)^{2}P$ + 27% $4f^{12}6s\ (^{1}D)^{2}D$ + 11% $5p^{4}4f^{14}6s\ (^{1}D)^{2}D$
109	483 654	483 589	508 172	486 471	3/2	35% $4f^{12}6s\ (^{3}P)^{2}P$ + 21% $5p^{4}4f^{14}6s\ (^{3}P)^{2}P$ + 19% $4f^{12}6s\ (^{1}D)^{2}D$
110	489 195	488 334	518 853	510 974	3/2	41% $5p^{4}4f^{14}5d\ (^{1}D)^{2}P$ + 22% $5p^{4}4f^{14}5d\ (^{3}P)^{2}P$ + 12% $5p^{4}4f^{14}5d\ (^{3}P)^{4}F$
111	493 723	493 431	527 411	520 070	5/2	44% $5p^{4}4f^{14}5d\ (^{3}P)^{2}D$ + 18% $5p^{4}4f^{14}5d\ (^{1}D)^{2}D$ + 18% $5p^{4}4f^{14}5d\ (^{1}D)^{2}F$
112	497 472	497 927	526 382	510 510	1/2	50% $5p^{4}4f^{14}6s\ (^{1}S)^{2}S$ + 30% $5p^{4}4f^{14}6s\ (^{3}P)^{4}P$ + 11% $5p^{4}4f^{14}6s\ (^{3}P)^{2}P$
113	504 584	505 392	534 257	530 547	1/2	37% $5p^{4}4f^{14}5d\ (^{1}D)^{2}P$ + 22% $5p^{4}4f^{14}5d\ (^{3}P)^{2}P$ + 17% $5p^{4}4f^{14}5d\ (^{1}D)^{2}S$
114	508 918	509 546	536 668	529 663	3/2	41% $5p^{4}4f^{14}5d\ (^{1}D)^{2}D$ + 22% $5p^{4}4f^{14}5d\ (^{3}P)^{2}D$ + 8% $5p^{4}4f^{14}5d\ (^{3}P)^{4}F$
115	519 141	519 306	521 058	519 960	7/2	58% $5p^{5}4f^{13}6s\ (^{3}D)^{4}D$ + 22% $5p54f^{13}6s\ (^{3}F)^{4}F$ + 11% $5p^{5}4f^{13}6s\ (^{1}F)^{2}F$
116	521 411	521 384	523 614	522 995	5/2	49% $5p^{5}4f^{13}6s\ (^{3}D)^{2}D$ + 14% $5p^{5}4f^{13}6s\ (^{3}F)^{4}F$ + 14% $5p^{5}4f^{13}6s\ (^{3}D)^{4}D$
117	522 954	523 014	525 169	524 042	7/2	41% $5p^{5}4f^{13}6s\ (^{1}G)^{2}G$ + 20% $5p54f^{13}6s\ (^{3}G)^{4}G$ + 19% $5p^{5}4f^{13}6s\ (^{3}F)^{2}F$
118	523 475	523 444	525 775	524 777	9/2	45% $5p^{5}4f136s\ (^{1}G)^{2}G$ + 25% $5p^{5}4f^{13}6s\ (^{3}G)^{4}G$ + 19% $5p^{5}4f^{13}6s\ (^{3}F)^{4}F$
119	530 756	530 423	560 745	555 257	1/2	42% $4f^{12}6s\ (^{1}S)^{2}S$ + 20% $5p^{4}4f^{14}5d\ (^{1}D)^{2}S$ + 11% $5p^{4}4f^{14}5d\ (^{3}P)^{2}P$
120	531 351	531 445	532 769	531 533	5/2	74% $5p^{5}4f^{13}6s\ (^{3}G)^{4}G$ + 18% $5p^{5}4f^{13}6s\ (^{1}F)^{2}F$ + 4% $5p^{5}4f^{13}6s\ (^{3}F)^{4}F$
121	533 310	533 231	535 013	533 867	7/2	49% $5p^{5}4f^{13}6s\ (^{3}G)^{2}G$ + 28% $5p^{5}4f^{13}6s\ (^{3}G)^{4}G$ + 16% $5p^{5}4f^{13}6s\ (^{1}F)^{2}F$
122	534 789	535 058	554 172	542 914	1/2	45% $4f^{12}6s\ (^{1}S)^{2}S$ + 19% $5p^{4}4f^{14}5d\ (^{1}D)^{2}S$ + 9% $5s4f^{14}\ (^{1}S)^{2}S$
123	537 266	537 296	540 675	538 685	5/2	35% $5p^{5}4f^{13}6s\ (^{1}D)^{2}D$ + 22% $5p^{5}4f^{13}6s\ (^{3}F)^{2}F$ + 16% $5p^{5}4f^{13}6s\ (^{3}D)^{4}D$
124	538 189	538 102	541 978	539 988	3/2	36% $5p^{5}4f^{13}6s\ (^{1}D)^{2}D$ + 31% $5p^{5}4f^{13}6s\ (^{3}F)^{4}F$ + 13% $5p^{5}4f^{13}6s\ (^{3}D)^{2}D$
125	550 802	550 970	574 058	560 305	3/2	81% $5p^{4}4f^{14}6s\ (^{3}P)^{4}P$ + 17% $5p^{4}4f^{14}6s\ (^{3}P)^{2}P$ + 1% $5p^{4}4f^{14}6s\ (^{1}D)^{2}D$
126	555 629	556 007	580 495	567 304	1/2	68% $5p^{4}4f^{14}6s\ (^{3}P)^{2}P$ + 31% $5p^{4}4f^{14}6s\ (^{3}P)^{4}P$ + 1% $5p^{4}4f^{14}6s\ (^{1}S)^{2}S$
127	568 591	568 680	599 793	593 594	3/2	31% $5p^{4}4f^{14}5d\ (^{1}S)^{2}D$ + 26% $5p^{4}4f^{14}5d\ (^{3}P)^{2}D$ + 11% $5p^{4}4f^{14}5d\ (^{3}P)^{2}P$
128	569 268	568 605	593 129	580 470	5/2	68% $5p^{4}4f^{14}6s\ (^{1}D)^{2}D$ + 18% $5p^{4}4f^{14}6s\ (^{3}P)^{4}P$ + 7% $5p^{5}4f^{13}6s\ (^{1}D)^{2}D$
129	571 235	570 198	594 875	582 191	3/2	59% $5p^{4}4f^{14}6s\ (^{1}D)^{2}D$ + 19% $5p^{4}4f^{14}6s\ (^{3}P)^{2}P$ + 6% $5p^{5}4f^{13}6s\ (^{1}D)^{2}D$
130	649 442	649 884	647 524	662 033	1/2	44% $5p^{4}4f^{14}6s\ (^{1}S)^{2}S$ + 31% $5p^{4}4f^{14}6s\ (^{3}P)^{4}P$ + 19% $5p^{4}4f^{14}6s\ (^{3}P)^{2}P$

[a] Experimental values from Ryabtsev et al. [5].
[b] Our HFR calculation.
[c] Our MCDHF-RCI-A calculation.
[d] Our MCDHF-RCI-B calculation.
[e] Our HFR calculation. At most, only the first three major components are given.

using the experimental wavelengths [5]. We also report the corresponding weighted Einstein A-coefficients as computed by Ryabtsev et al. [5] using the same HFR method but with more limited CI expansions. The uncertainty indicators as defined by NIST [10], $Unc.$, are also given for our two MCDHF models and for the HFR model of Ryabtsev et al. [5] and were evaluated using our HFR rates as reference values following the procedure described by Kramida [11].

Fig. 4 shows the logarithm of the ratio of the weighted Einstein coefficient determined by Ryabtsev et al. [5] to our HFR value, $log(gA_{RYA}/gA_{HFR})$, as a function of the line strength deduced from the former in a logarithmic scale, $log(S_{RYA})$. In Figs. 5 and 6, the same kind of plots have been drawn for our MCDHF-RCI-A and MCDHF-RCI-B models respectively using our HFR calculations as reference. These three figures have been employed to evaluate the uncertainty indicator, $Unc.$, as defined in NIST [10] and presented in Table 3. In Fig. 4,

Table 3
Comparison between the present calculated and the literature transition rates in Ta VII.

λ[a] (Å)	i[b]	k[b]	HFR[c] gA (s^{-1})	HFR[c] $log\ gf$	HFR[c] CF[g]	RCI-A[d] gA[i] (s^{-1})	RCI-A[d] $log\ gf$[i]	RCI-A[d] dT[j]	RCI-A[d] $Unc.$[h]	RCI-B[e] gA[i] (s^{-1})	RCI-B[e] $log\ gf$[i]	RCI-B[e] dT[j]	RCI-B[e] $Unc.$[h]	RYA[f] gA (s^{-1})	RYA[f] $Unc.$[h]
191.031	1	118	2.50E+11	0.14	0.88	1.03E+11	−0.25	0.04	E	1.32E+11	−0.14	0.02	E	2.55E+11	D
191.221	1	117	9.13E+10	−0.30	0.56	3.36E+10	−0.73	0.03	E	3.45E+10	−0.72	0.05	E	1.03E+11	D
191.283	2	124	9.93E+10	−0.26	0.93	8.83E+10	−0.32	0.04	E	6.07E+10	−0.48	0.03	E	1.01E+11	D
191.613	2	123	7.53E+10	−0.38	0.65	2.92E+10	−0.79	0.04	E	3.05E+10	−0.77	0.03	E	8.03E+10	D
191.784	1	116	1.62E+11	−0.05	0.76	8.69E+10	−0.32	0.05	E	1.11E+11	−0.21	0.03	E	1.66E+11	D
192.626	1	115	5.39E+10	−0.52	0.87	1.86E+10	−0.99	0.04	E	1.88E+10	−0.98	0.05	E	4.59E+10	E
193.076	2	121	1.90E+11	0.03	0.79	7.29E+10	−0.39	0.05	E	9.85E+10	−0.26	0.01	E	1.95E+11	D
193.809	2	120	3.82E+10	−0.67	0.78	1.54E+10	−1.06	0.05	E	1.48E+10	−1.08	0.05	E	3.62E+10	E
194.072	4	130	5.25E+10	−0.53	0.54	5.47E+07	−3.51	0.53	E	2.48E+10	−0.85	0.09	E	4.92E+10	E
194.660	3	129	2.28E+10	−0.89	0.05	1.02E+10	−1.24	0.07	E	7.51E+09	−1.37	0.19	E	2.25E+10	E
195.406	3	128	1.18E+11	−0.17	0.40	4.42E+10	−0.60	0.08	E	5.83E+10	−0.48	0.05	E	1.20E+11	D
197.016	2	117	3.01E+09	−1.76	0.01	1.65E+09	−2.02	0.03	E	2.33E+09	−1.87	0.13	E	2.60E+09	E
200.756	3	126	4.09E+10	−0.61	0.44	3.15E+10	−0.72	0.05	E	2.98E+09	−1.74	0.40	E	3.88E+10	E
202.547	1	111	4.61E+10	−0.55	0.25	3.90E+10	−0.62	0.03	E	7.61E+09	−1.33	0.13	E	4.52E+10	E
202.623	2	114	3.89E+10	−0.62	0.24	1.01E+10	−1.20	0.03	E	1.29E+10	−1.10	0.08	E	3.55E+10	E
202.721	3	125	6.33E+10	−0.41	0.73	3.46E+10	−0.67	0.07	E	3.35E+10	−0.69	0.09	E	6.06E+10	E
208.048	3	124	3.24E+09	−1.68	0.12	4.31E+09	−1.55	0.07	E	2.16E+09	−1.85	0.06	E	3.10E+09	E
208.440	3	123	1.10E+10	−1.15	0.47	8.12E+08	−2.28	0.14	E	2.43E+09	−1.80	0.26	E	9.80E+09	E
208.899	1	107	8.79E+09	−1.24	0.44	1.39E+09	−2.04	0.09	E	1.76E+10	−0.94	0.10	E	6.80E+09	E
209.052	2	111	1.34E+10	−1.06	0.33	3.35E+09	−1.66	0.12	E	6.64E+09	−1.36	0.14	E	1.05E+10	E
209.523	3	122	4.87E+10	−0.50	0.08	6.13E+08	−2.39	0.41	E	1.16E+09	−2.12	0.35	E	2.17E+10	E
211.053	2	110	7.45E+08	−2.30	0.12	6.41E+08	−2.37	0.05	E	9.21E+08	−2.21	0.11	E	1.00E+09	E
211.170	1	106	2.11E+10	−0.85	0.28	1.47E+10	−1.01	0.09	E	1.34E+10	−1.05	0.10	E	1.89E+10	E
211.309	3	119	4.50E+10	−0.52	0.07	2.18E+10	−0.84	0.13	E	5.09E+10	−0.47	0.13	E	6.57E+10	D
213.201	1	105	1.94E+09	−1.88	0.00	1.58E+06	−4.97	0.71	E	8.41E+08	−2.24	0.16	E	2.40E+09	E
213.304	1	104	2.98E+10	−0.69	0.04	1.52E+10	−0.98	0.12	E	1.88E+10	−0.89	0.13	E	3.09E+10	E
213.986	1	103	1.77E+10	−0.91	0.09	8.44E+09	−1.24	0.09	E	2.57E+10	−0.75	0.01	E	1.98E+10	E
214.038	2	108	3.89E+09	−1.57	0.51	8.68E+07	−3.22	0.11	E	5.23E+09	−1.45	0.06	E	2.70E+09	E
215.567	3	116	2.96E+09	−1.69	0.62	5.34E+10	−0.43	0.12	E	1.45E+11	0.01	0.05	E	3.10E+09	E
215.836	2	107	8.39E+09	−1.23	0.37	8.46E+08	−2.23	0.13	E	1.62E+10	−0.95	0.11	E	5.70E+09	E
217.050	1	99	2.59E+10	−0.74	0.88	5.23E+08	−2.43	0.12	E	8.67E+09	−1.21	0.05	E	2.23E+10	E
217.753	1	98	1.11E+09	−2.10	0.12	4.91E+11	0.54	0.09	E	1.02E+09	−2.14	0.13	E	6.10E+09	E
218.260	2	106	1.93E+10	−0.86	0.28	4.41E+09	−1.50	0.15	E	1.67E+11	0.08	0.12	E	1.41E+10	E
219.187	1	96	5.28E+10	−0.42	0.35	1.87E+10	−0.87	0.10	E	3.44E+11	0.39	0.11	E	4.83E+10	E
219.246	1	95	3.68E+11	0.42	0.73	1.81E+12	1.11	0.09	E	8.33E+11	0.78	0.10	E	3.56E+11	D+
220.335	1	94	2.18E+12	1.20	0.87	3.93E+10	−0.54	0.09	E	1.55E+12	1.05	0.11	D	2.17E+12	AA
220.388	1	93	3.51E+10	−0.59	0.21	1.92E+06	−4.86	0.62	E	3.82E+08	−2.56	0.04	E	4.14E+10	E
220.428	2	105	1.91E+12	1.14	0.88	9.79E+11	0.85	0.09	E	1.28E+12	0.97	0.10	D	1.92E+12	AAA
220.538	2	104	1.99E+12	1.16	0.86	6.21E+11	0.66	0.06	E	1.84E+12	1.13	0.08	B	1.99E+12	AA
221.529	3	114	2.15E+11	0.20	0.43	3.51E+11	0.41	0.09	E	3.59E+11	0.42	0.06	E	2.51E+11	D+
221.595	1	91	1.95E+12	1.16	0.91	2.36E+12	1.24	0.10	C	1.49E+12	1.04	0.11	D+	1.94E+12	AA
221.885	2	102	1.15E+12	0.93	0.91	1.75E+12	1.11	0.10	E	1.21E+12	0.95	0.11	D+	1.22E+12	B
221.928	1	90	6.84E+10	−0.30	0.37	2.12E+08	−2.81	0.07	E	1.17E+10	−1.06	0.14	E	7.95E+10	D
222.022	1	89	3.25E+12	1.38	0.92	2.26E+12	1.22	0.07	D	2.92E+12	1.33	0.08	C+	3.24E+12	AA
222.327	1	88	3.31E+09	−1.61	0.13	4.42E+07	−3.48	0.49	E	1.17E+09	−2.06	0.03	E	4.20E+09	E
223.045	1	87	1.18E+09	−2.06	0.07	7.83E+07	−3.23	0.05	E	8.55E+08	−2.20	0.08	E	1.10E+09	E
223.613	1	86	5.38E+09	−1.39	0.03	2.58E+08	−2.71	0.07	E	2.95E+09	−1.66	0.12	E	3.20E+09	E
223.671	3	113	5.55E+11	0.62	0.69	1.08E+12	0.91	0.10	E	5.45E+11	0.61	0.12	E	6.13E+11	C
223.719	2	101	4.24E+09	−1.50	0.06	4.50E+11	0.53	0.09	E	2.94E+10	−0.66	0.08	E	2.70E+09	E
224.282	2	100	2.33E+10	−0.76	0.20	1.84E+10	−0.86	0.10	E	3.85E+10	−0.54	0.02	E	2.20E+10	E
224.544	2	99	3.24E+11	0.39	0.89	1.09E+12	0.92	0.08	E	6.22E+10	−0.33	0.01	E	2.60E+11	D+
225.287	2	98	4.55E+10	−0.46	0.81	1.23E+09	−2.03	0.21	E	2.08E+08	−2.80	0.28	E	1.17E+11	E
225.318	2	97	2.85E+10	−0.67	0.51	8.77E+09	−1.18	0.08	E	1.77E+07	−3.87	0.21	E	2.40E+10	E
226.830	2	96	9.21E+10	−0.15	0.44	1.80E+11	0.14	0.09	E	4.59E+10	−0.45	0.07	E	9.03E+10	D
226.894	2	95	3.70E+11	0.46	0.37	6.98E+09	−1.27	0.01	E	4.48E+11	0.54	0.08	E	3.49E+11	D+
227.294	3	112	6.71E+10	−0.29	0.78	8.54E+10	−0.18	0.10	E	3.66E+10	−0.55	0.01	E	6.54E+10	D
227.370	1	85	1.55E+11	0.08	0.52	1.12E+11	−0.06	0.05	E	1.39E+11	0.03	0.00	E	1.52E+11	D
228.059	2	94	2.11E+10	−0.79	0.06	2.66E+06	−4.68	0.96	E	1.18E+11	−0.04	0.11	E	1.76E+10	E
228.118	2	93	4.98E+10	−0.41	0.24	1.50E+10	−0.93	0.06	E	7.60E+10	−0.23	0.02	E	5.17E+10	D
228.194	2	92	1.83E+10	−0.84	0.73	4.39E+10	−0.46	0.04	E	6.63E+09	−1.29	0.03	E	1.65E+10	E
228.234	1	84	1.34E+10	−0.98	0.02	1.31E+10	−1.00	0.06	E	2.05E+10	−0.80	0.08	E	1.53E+09	E
228.379	1	83	1.87E+11	0.16	0.56	1.47E+11	0.06	0.05	E	1.47E+11	0.06	0.01	E	1.93E+11	E
228.797	4	129	1.19E+09	−2.03	0.00	1.24E+10	−1.01	0.04	E	5.53E+10	−0.36	0.03	E	1.33E+10	E
228.884	1	82	1.01E+10	−1.10	0.09	3.68E+09	−1.54	0.06	E	2.19E+09	−1.76	0.08	E	9.19E+09	E
229.246	3	111	1.50E+12	1.07	0.81	9.07E+11	0.85	0.10	E	1.34E+12	1.02	0.06	C+	1.60E+12	B+
229.405	2	91	2.93E+09	−1.64	0.01	6.93E+09	−1.26	0.07	E	2.40E+10	−0.72	0.09	E	2.50E+09	E
229.462	1	81	3.43E+10	−0.57	0.32	3.19E+10	−0.60	0.05	E	2.37E+10	−0.73	0.04	E	3.19E+10	E
229.771	2	90	6.13E+05	−5.32	0.00	4.40E+10	−0.46	0.04	E	9.83E+08	−2.11	0.11	E	2.00E+08	E

(*continued on next page*)

Table 3 (*continued*).

λ[a]	i[b]	k[b]	HFR[c]			RCI-A[d]				RCI-B[e]				RYA[f]	
(Å)			gA (s^{-1})	$log\ gf$	CF[g]	gA[i] (s^{-1})	$log\ gf$[i]	dT[j]	$Unc.$[h]	gA[i] (s^{-1})	$log\ gf$[i]	dT[j]	$Unc.$[h]	gA (s^{-1})	$Unc.$[h]
229.906	1	80	2.07E+09	−1.79	0.01	1.43E+11	0.05	0.05	E	2.52E+09	−1.70	0.11	E	3.04E+09	E
230.191	4	127	9.97E+11	0.90	0.83	4.65E+11	0.57	0.10	E	9.25E+11	0.87	0.07	D	1.05E+12	C+
230.205	2	88	2.70E+10	−0.67	0.48	6.62E+10	−0.28	0.04	E	3.31E+07	−3.58	0.55	E	1.77E+10	E
230.970	2	87	2.34E+10	−0.73	0.42	2.79E+08	−2.65	0.06	E	1.64E+10	−0.88	0.00	E	2.64E+10	E
231.574	2	86	1.32E+10	−0.98	0.20	2.24E+05	−5.74	0.77	E	1.20E+10	−1.02	0.00	E	1.28E+10	E
231.652	3	110	8.13E+11	0.82	0.79	5.72E+11	0.66	0.10	E	5.60E+11	0.65	0.09	E	7.59E+11	C+
231.702	1	79	5.05E+08	−2.39	0.00	3.00E+08	−2.62	0.11	E	6.55E+08	−2.28	0.05	E	5.50E+08	E
232.999	1	78	7.95E+09	−1.19	0.02	1.52E+09	−1.91	0.12	E	7.47E+08	−2.22	0.20	E	6.20E+09	E
234.199	1	77	1.19E+10	−1.01	0.06	4.09E+09	−1.47	0.06	E	5.40E+09	−1.35	0.05	E	1.20E+10	E
234.664	3	109	4.89E+10	−0.39	0.55	7.76E+10	−0.19	0.04	E	7.13E+08	−2.23	0.21	E	4.70E+10	D
235.257	3	108	2.88E+10	−0.62	0.14	5.58E+08	−2.33	0.13	E	8.34E+10	−0.16	0.09	E	2.49E+10	E
236.654	1	75	1.92E+08	−2.79	0.00	2.33E+07	−3.71	0.36	E	8.18E+08	−2.16	0.04	E	1.23E+09	E
236.694	2	83	2.16E+09	−1.74	0.01	2.02E+09	−2.02	0.05	E	1.01E+09	−2.07	0.15	E	1.53E+09	E
237.233	2	82	2.56E+09	−1.67	0.01	4.72E+09	−1.40	0.07	E	1.27E+09	−1.97	0.06	E	1.49E+09	E
237.271	4	126	7.15E+10	−0.22	0.79	1.18E+11	0.00	0.08	E	2.05E+11	0.24	0.04	E	6.62E+10	D
237.426	3	107	8.50E+09	−1.14	0.03	2.89E+09	−1.61	0.05	E	2.55E+08	−2.67	0.47	E	1.07E+10	E
237.723	1	73	1.90E+08	−2.79	0.00	1.91E+09	−1.79	0.03	E	3.30E+05	−5.55	0.35	E	5.20E+08	E
237.862	2	81	1.74E+09	−1.83	0.01	2.46E+09	−1.68	0.05	E	2.03E+09	−1.76	0.09	E	1.70E+09	E
238.331	2	80	2.83E+09	−1.62	0.03	8.41E+08	−2.15	0.05	E	2.46E+09	−1.68	0.00	E	2.34E+09	E
239.195	1	71	8.55E+09	−1.13	0.01	4.50E+09	−1.41	0.12	E	4.67E+09	−1.40	0.11	E	7.22E+09	E
240.264	2	79	8.33E+09	−1.14	0.02	3.24E+09	−1.55	0.09	E	1.11E+09	−2.02	0.14	E	7.69E+09	E
240.363	3	106	5.20E+10	−0.35	0.10	2.05E+10	−0.75	0.14	E	4.53E+10	−0.41	0.04	E	4.42E+10	D
240.486	1	69	9.47E+09	−1.08	0.02	1.24E+09	−1.97	0.17	E	4.47E+09	−1.41	0.09	E	9.02E+09	E
241.465	1	68	5.19E+08	−2.34	0.00	1.92E+08	−2.77	0.07	E	7.90E+08	−2.16	0.40	E	3.40E+08	E
242.950	2	77	1.04E+10	−1.03	0.06	1.19E+09	−1.98	0.10	E	4.30E+09	−1.42	0.07	E	9.93E+09	E
243.000	3	105	1.73E+10	−0.82	0.12	1.58E+10	−0.85	0.10	E	5.15E+06	−4.34	0.45	E	1.48E+10	E
244.674	1	65	1.88E+10	−0.77	0.03	1.08E+10	−1.01	0.09	E	1.44E+10	−0.89	0.09	E	2.11E+10	E
245.059	2	76	2.77E+07	−3.60	0.00	1.03E+09	−2.03	0.10	E	1.57E+08	−2.85	0.14	E	1.20E+08	E
245.590	2	75	1.72E+10	−0.81	0.03	6.61E+08	−2.22	0.03	E	6.66E+09	−1.22	0.10	E	2.22E+10	E
246.747	2	73	2.47E+09	−1.65	0.01	1.24E+09	−1.95	0.03	E	7.20E+09	−1.18	0.09	E	1.46E+09	E
247.004	3	101	9.31E+09	−1.07	0.53	6.28E+07	−3.24	0.30	E	9.51E+09	−1.06	0.08	E	1.02E+10	E
247.525	4	124	2.20E+09	−1.70	0.15	2.28E+09	−1.68	0.03	E	5.69E+09	−1.28	0.16	E	1.80E+09	E
248.169	2	72	1.71E+09	−1.80	0.01	6.04E+08	−2.25	0.08	E	2.27E+07	−3.68	0.27	E	2.74E+09	E
248.321	2	71	3.07E+09	−1.55	0.01	1.61E+09	−1.83	0.09	E	1.92E+09	−1.75	0.12	E	2.84E+09	E
248.572	1	63	1.46E+10	−0.87	0.03	1.81E+10	−0.78	0.13	E	1.26E+10	−0.93	0.14	E	1.29E+10	E
249.613	4	122	2.17E+11	0.31	0.71	2.11E+10	−0.71	0.05	E	1.06E+10	−1.00	0.12	E	1.11E+11	E
249.721	2	69	2.75E+09	−1.59	0.00	1.60E+10	−0.82	0.07	E	4.77E+08	−2.35	0.31	E	1.75E+09	E
250.806	3	96	7.87E+10	−0.13	0.16	1.81E+10	−0.77	0.10	E	3.79E+10	−0.45	0.06	E	7.41E+10	D
252.151	4	119	2.29E+11	0.34	0.67	3.46E+11	0.52	0.11	E	2.81E+11	0.43	0.13	E	3.63E+11	E
252.197	2	67	2.21E+10	−0.68	0.13	2.52E+09	−1.62	0.09	E	2.11E+10	−0.70	0.15	E	1.89E+10	E
252.376	3	93	6.61E+09	−1.20	0.12	5.14E+07	−3.31	0.45	E	2.66E+07	−3.60	0.24	E	5.90E+09	E
252.471	3	92	5.55E+08	−2.27	0.19	1.91E+08	−2.74	0.17	E	6.43E+08	−2.21	0.15	E	3.00E+08	E
254.921	3	88	1.83E+09	−1.75	0.13	2.60E+07	−3.60	0.23	E	7.62E+07	−3.13	0.02	E	1.10E+09	E
255.262	1	61	1.21E+09	−1.93	0.01	2.45E+09	−1.62	0.09	E	4.98E+10	−0.31	0.09	E	7.80E+08	E
255.861	3	87	1.66E+09	−1.79	0.38	2.10E+07	−3.69	0.36	E	1.36E+09	−1.87	0.01	E	1.50E+09	E
257.007	1	59	1.87E+10	−0.73	0.11	3.17E+09	−1.50	0.02	E	3.02E+09	−1.52	0.22	E	1.93E+10	E
258.448	2	63	3.68E+08	−2.43	0.00	1.66E+09	−1.78	0.10	E	1.71E+09	−1.77	0.11	E	1.60E+08	E
262.438	1	57	2.27E+10	−0.63	0.45	5.55E+08	−2.24	0.23	E	1.06E+09	−1.96	0.22	E	2.89E+10	E
262.727	1	56	9.53E+09	−1.01	0.26	1.75E+06	−4.74	0.83	E	9.07E+08	−2.03	0.13	E	1.15E+10	E
263.030	2	62	1.07E+10	−0.96	0.31	2.58E+10	−0.57	0.14	E	1.49E+10	−0.81	0.11	E	8.29E+09	E
263.574	3	82	7.92E+09	−1.09	0.07	4.69E+10	−0.31	0.16	E	1.78E+10	−0.73	0.14	E	6.95E+09	E
265.126	1	55	3.48E+11	0.57	0.62	9.32E+09	−1.01	0.10	E	2.72E+11	0.46	0.09	E	3.49E+11	C
265.700	2	61	2.83E+11	0.48	0.67	1.77E+11	0.27	0.09	E	4.52E+08	−2.32	0.24	E	2.83E+11	D+
266.148	2	60	5.50E+10	−0.23	0.79	4.20E+10	−0.35	0.10	E	7.37E+10	−0.11	0.10	E	7.95E+10	D
266.844	4	114	2.57E+11	0.44	0.34	6.36E+10	−0.17	0.10	E	1.25E+11	0.12	0.05	E	2.45E+11	D+
267.103	1	52	3.98E+09	−1.37	0.17	7.53E+08	−2.09	0.16	E	2.51E+10	−0.57	0.08	E	1.08E+10	E
267.238	1	51	1.61E+11	0.24	0.38	5.90E+09	−1.20	0.10	E	1.51E+09	−1.79	0.11	E	1.70E+11	D+
267.311	1	50	1.79E+10	−0.72	0.22	9.74E+10	0.02	0.08	E	1.03E+10	−0.96	0.04	E	1.14E+10	E
267.588	2	59	3.17E+11	0.53	0.51	1.56E+10	−0.78	0.12	E	1.48E+11	0.20	0.06	E	3.27E+11	C
267.863	1	49	4.04E+11	0.64	0.89	2.07E+11	0.35	0.06	E	2.62E+11	0.45	0.06	E	4.04E+11	C
269.214	2	58	7.23E+10	−0.11	0.63	5.13E+10	−0.25	0.10	E	1.40E+09	−1.82	0.22	E	5.29E+10	D
269.738	1	48	9.08E+09	−1.01	0.09	1.49E+11	0.21	0.08	E	9.61E+08	−1.98	0.06	E	6.84E+09	E
269.788	1	47	7.93E+09	−1.06	0.09	7.76E+09	−1.07	0.11	E	3.31E+10	−0.44	0.10	E	8.69E+09	E
269.973	4	113	3.23E+10	−0.45	0.07	1.26E+08	−2.86	0.05	E	5.80E+09	−1.20	0.06	E	1.27E+10	E
270.642	3	77	2.18E+10	−0.62	0.45	3.80E+10	−0.38	0.05	E	2.80E+10	−0.51	0.15	E	2.09E+10	E
271.046	1	46	1.16E+10	−0.89	0.12	7.30E+10	−0.09	0.10	E	4.42E+10	−0.31	0.10	E	9.64E+09	E
272.889	1	45	1.20E+10	−0.87	0.06	1.18E+10	−0.88	0.05	E	8.12E+09	−1.04	0.02	E	6.66E+09	E
273.270	3	76	9.35E+09	−0.98	0.16	5.34E+09	−1.22	0.11	E	4.75E+09	−1.27	0.25	E	6.41E+09	E
273.474	2	57	3.17E+10	−0.45	0.34	3.46E+10	−0.41	0.07	E	1.03E+10	−0.94	0.03	E	2.74E+10	D

(continued on next page)

Table 3 (*continued*).

λ[a]	i[b]	k[b]	HFR[c]			RCI-A[d]				RCI-B[e]				RYA[f]	
(Å)			gA (s−1)	log gf	CF[g]	gA[i] (s−1)	log gf[i]	dT[j]	Unc.[h]	gA[i] (s−1)	log gf[i]	dT[j]	Unc.[h]	gA (s−1)	Unc.[h]
273.929	3	75	1.10E+10	−0.91	0.16	5.25E+04	−6.23	0.95	E	1.51E+10	−0.77	0.09	E	1.40E+10	E
274.279	1	44	3.36E+09	−1.42	0.01	2.04E+09	−1.64	0.13	E	1.03E+09	−1.93	0.07	E	3.20E+09	E
274.455	1	43	1.56E+10	−0.75	0.10	4.96E+10	−0.25	0.09	E	1.48E+10	−0.78	0.08	E	1.50E+10	E
275.252	4	112	5.08E+08	−2.24	0.01	3.22E+08	−2.44	0.42	E	4.89E+08	−2.26	0.36	E	8.00E+08	E
275.284	3	74	3.26E+09	−1.43	0.06	3.50E+10	−0.40	0.08	E	1.94E+09	−1.66	0.13	E	4.32E+09	E
275.365	3	73	1.03E+09	−1.93	0.07	2.37E+09	−1.57	0.07	E	9.97E+09	−0.95	0.09	E	7.00E+07	E
275.464	1	41	4.13E+08	−2.33	0.00	5.92E+09	−1.17	0.04	E	1.75E+09	−1.70	0.12	E	3.90E+08	E
276.388	2	55	4.70E+09	−1.27	0.02	1.12E+11	0.11	0.05	E	6.05E+09	−1.16	0.03	E	4.21E+09	E
276.521	1	39	2.98E+09	−1.47	0.03	3.11E+09	−1.45	0.10	E	1.28E+09	−1.83	0.09	E	2.13E+09	E
277.144	3	72	4.12E+10	−0.32	0.35	3.33E+10	−0.42	0.07	E	3.65E+10	−0.38	0.04	E	3.66E+10	D
277.626	2	54	1.77E+09	−1.69	0.05	4.90E+05	−5.25	0.58	E	4.75E+08	−2.26	0.13	E	2.04E+09	E
278.422	1	38	2.81E+09	−1.49	0.02	1.41E+09	−1.79	0.14	E	1.80E+09	−1.68	0.10	E	3.09E+09	E
278.779	2	50	2.62E+09	−1.51	0.09	2.58E+09	−1.52	0.04	E	7.89E+10	−0.04	0.09	E	2.38E+09	E
278.957	3	70	9.83E+08	−1.94	0.01	5.83E+08	−2.17	0.35	E	1.89E+09	−1.66	0.04	E	1.61E+09	E
279.083	3	69	5.38E+10	−0.20	0.49	1.92E+09	−1.65	0.27	E	4.82E+08	−2.25	0.07	E	4.61E+10	D
280.408	3	68	1.46E+11	0.24	0.77	2.26E+08	−2.57	0.24	E	2.70E+07	−3.50	0.54	E	1.61E+11	D+
281.420	2	48	1.02E+08	−2.92	0.00	2.15E+09	−1.59	0.03	E	5.14E+06	−4.21	0.24	E	8.00E+07	E
281.484	2	47	8.72E+08	−1.99	0.01	4.34E+08	−2.29	0.20	E	2.84E+07	−3.47	0.00	E	6.60E+08	E
281.670	4	110	3.81E+10	−0.34	0.17	2.56E+10	−0.52	0.09	E	5.04E+10	−0.22	0.09	E	3.81E+10	D
281.892	1	36	1.16E+10	−0.86	0.05	1.67E+10	−0.70	0.09	E	2.69E+08	−2.49	0.00	E	1.25E+10	E
282.168	3	67	1.45E+08	−2.76	0.00	9.99E+06	−3.92	0.02	E	2.29E+07	−3.56	0.38	E	3.70E+08	E
282.867	1	34	2.49E+09	−1.53	0.01	5.14E+09	−1.21	0.12	E	1.37E+10	−0.79	0.14	E	3.05E+09	E
283.107	1	33	8.12E+08	−2.01	0.00	3.91E+08	−2.33	0.19	E	9.72E+08	−1.93	0.15	E	1.06E+09	E
283.377	1	32	9.61E+09	−0.94	0.04	7.43E+08	−2.05	0.08	E	9.92E+09	−0.92	0.13	E	9.35E+09	E
283.892	1	31	6.23E+08	−2.12	0.00	5.80E+09	−1.15	0.10	E	5.85E+07	−3.15	0.18	E	2.20E+08	E
284.359	1	29	2.01E+10	−0.61	0.03	1.47E+10	−0.75	0.14	E	4.40E+08	−2.27	0.67	E	2.10E+10	E
284.469	3	66	9.31E+10	0.05	0.44	2.92E+09	−1.45	0.22	E	3.46E+10	−0.38	0.03	E	9.39E+10	D+
284.797	3	64	3.22E+10	−0.41	0.26	1.82E+09	−1.66	0.17	E	1.06E+08	−2.89	0.84	E	4.08E+10	D
285.849	1	28	2.21E+09	−1.57	0.01	6.37E+08	−2.11	0.33	E	1.21E+09	−1.83	0.12	E	2.60E+09	E
286.371	2	44	1.42E+09	−1.76	0.00	3.45E+06	−4.37	0.69	E	1.67E+09	−1.69	0.18	E	8.10E+08	E
286.418	1	26	1.52E+09	−1.73	0.01	2.52E+06	−4.51	0.15	E	1.97E+09	−1.62	0.02	E	1.08E+09	E
286.540	2	43	3.39E+08	−2.38	0.01	2.35E+08	−2.54	0.14	E	3.50E+08	−2.37	0.08	E	2.10E+08	E
286.758	1	25	1.67E+09	−1.69	0.01	2.45E+08	−2.52	0.40	E	1.97E+07	−3.61	0.76	E	2.03E+09	E
287.015	4	108	4.80E+08	−2.23	0.01	2.21E+07	−3.56	0.58	E	1.23E+08	−2.82	0.56	E	4.00E+08	E
287.169	2	42	6.81E+09	−1.08	0.10	1.47E+10	−0.74	0.10	E	5.38E+09	−1.18	0.16	E	8.13E+09	E
287.641	2	41	1.40E+09	−1.76	0.00	2.66E+07	−3.48	0.98	E	4.79E+08	−2.23	0.06	E	4.80E+08	E
288.126	1	23	3.01E+09	−1.43	0.01	4.91E+09	−1.21	0.03	E	2.99E+09	−1.43	0.07	E	2.22E+09	E
288.722	2	40	3.59E+09	−1.35	0.05	3.60E+09	−1.35	0.11	E	1.32E+09	−1.78	0.20	E	2.81E+09	E
288.807	2	39	4.21E+09	−1.28	0.02	2.80E+08	−2.46	0.31	E	1.47E+09	−1.74	0.18	E	3.37E+09	E
289.146	1	20	1.53E+09	−1.72	0.00	1.72E+04	−6.67	0.89	E	4.91E+06	−4.21	0.79	E	1.58E+09	E
289.898	1	19	5.67E+09	−1.15	0.02	8.32E+08	−1.98	0.05	E	3.01E+07	−3.42	0.62	E	5.76E+09	E
290.041	3	63	2.40E+09	−1.52	0.04	4.83E+05	−5.21	0.85	E	1.67E+08	−2.68	0.35	E	2.09E+09	E
290.244	1	18	4.62E+09	−1.23	0.01	5.12E+06	−4.19	0.77	E	7.27E+08	−2.04	0.07	E	3.27E+09	E
290.588	1	17	1.49E+08	−2.73	0.00	3.11E+09	−1.40	0.02	E	1.90E+09	−1.62	0.02	E	5.60E+08	E
290.711	1	16	4.99E+08	−2.20	0.01	1.28E+09	−1.79	0.00	E	1.05E+09	−1.88	0.10	E	6.00E+08	E
290.875	2	38	1.35E+09	−1.77	0.00	3.97E+09	−1.30	0.17	E	1.43E+09	−1.74	0.61	E	3.27E+09	E
291.991	1	15	4.96E+09	−1.20	0.02	1.79E+09	−1.64	0.13	E	4.00E+09	−1.29	0.29	E	5.99E+09	E
292.631	1	14	1.72E+09	−1.66	0.01	9.67E+07	−2.91	0.42	E	8.58E+09	−0.96	0.11	E	1.60E+09	E
294.055	2	37	9.46E+08	−1.91	0.01	2.13E+09	−1.56	0.16	E	1.19E+09	−1.81	0.32	E	1.10E+09	E
294.269	1	12	4.98E+08	−2.19	0.00	1.19E+06	−4.81	0.75	E	1.67E+09	−1.66	0.40	E	7.30E+08	E
294.618	1	11	1.92E+09	−1.60	0.01	8.11E+08	−1.98	0.24	E	1.28E+08	−2.78	0.83	E	1.30E+09	E
294.667	2	36	5.56E+08	−2.14	0.00	1.09E+09	−1.85	0.19	E	1.86E+09	−1.62	0.12	E	6.60E+08	E
295.257	2	35	9.15E+08	−1.92	0.01	1.27E+09	−1.78	0.17	E	6.42E+08	−2.08	0.34	E	2.18E+09	E
295.994	2	33	4.87E+09	−1.19	0.01	7.83E+07	−2.99	0.02	E	1.83E+09	−1.62	0.39	E	4.92E+09	E
296.849	2	31	7.52E+08	−2.00	0.00	6.37E+06	−4.08	0.12	E	2.76E+07	−3.44	0.35	E	3.40E+08	E
297.014	1	10	2.33E+08	−2.51	0.00	2.80E+09	−1.43	0.11	E	1.26E+08	−2.78	0.32	E	1.29E+09	E
297.099	2	30	3.06E+09	−1.39	0.03	2.25E+08	−2.53	0.00	E	1.50E+09	−1.70	0.32	E	3.58E+09	E
297.924	1	9	3.90E+09	−1.29	0.02	1.51E+09	−1.70	0.12	E	4.88E+05	−5.19	0.98	E	3.86E+09	E
298.993	2	28	1.79E+08	−2.62	0.00	1.05E+08	−2.85	0.85	E	4.85E+08	−2.19	0.42	E	9.00E+07	E
299.197	3	61	1.30E+09	−1.76	0.18	1.54E+08	−2.69	0.36	E	4.33E+05	−5.24	1.00	E	1.38E+09	E
299.281	2	27	1.11E+08	−2.83	0.00	5.45E+07	−3.14	0.12	E	2.04E+08	−2.56	0.44	E	6.00E+07	E
299.769	3	60	3.83E+09	−1.29	0.04	2.45E+08	−2.48	0.29	E	2.79E+08	−2.43	0.09	E	2.00E+09	E
300.523	2	24	1.04E+08	−2.85	0.00	6.78E+08	−2.04	0.10	E	3.61E+05	−5.31	0.90	E	9.00E+07	E
301.482	2	23	1.46E+08	−2.70	0.00	5.82E+07	−3.10	0.54	E	9.55E+07	−2.89	0.79	E	1.80E+08	E
302.613	2	20	2.02E+07	−3.55	0.00	2.01E+06	−4.56	0.81	E	4.55E+07	−3.20	0.65	E	1.60E+08	E
303.668	3	58	2.46E+09	−1.47	0.03	2.47E+08	−2.47	0.07	E	3.63E+09	−1.30	0.23	E	2.52E+09	E
304.181	2	17	2.08E+09	−1.54	0.02	2.64E+08	−2.44	0.17	E	1.58E+09	−1.66	0.22	E	2.93E+09	E
304.316	2	16	3.04E+08	−2.38	0.00	2.43E+04	−6.47	1.00	E	9.24E+07	−2.89	0.62	E	2.10E+08	E
306.427	2	14	7.47E+08	−1.98	0.00	5.39E+08	−2.12	0.04	E	6.03E+06	−4.07	0.82	E	4.90E+08	E
307.212	2	13	7.83E+07	−2.96	0.00	4.54E+08	−2.19	0.31	E	1.26E+08	−2.75	0.66	E	7.00E+07	E
307.663	4	97	3.66E+09	−1.29	0.02	3.04E+08	−2.36	0.06	E	2.38E+09	−1.47	0.19	E	3.80E+09	E
308.218	2	12	1.13E+08	−2.80	0.00	1.12E+06	−4.80	0.86	E	6.31E+07	−3.05	0.01	E	1.00E+07	E
309.381	1	8	1.33E+08	−2.72	0.00	8.11E+06	−3.93	0.60	E	1.88E+08	−2.57	0.07	E	1.10E+08	E

(*continued on next page*)

Table 3 (*continued*).

λ[a] (Å)	i[b]	k[b]	HFR[c]			RCI-A[d]				RCI-B[e]				RYA[f]	
			gA (s^{-1})	$log\ gf$	CF[g]	gA[i] (s^{-1})	$log\ gf$[i]	dT[j]	$Unc.$[h]	gA[i] (s^{-1})	$log\ gf$[i]	dT[j]	$Unc.$[h]	gA (s^{-1})	$Unc.$[h]
309.519	1	7	1.39E+08	−2.70	0.00	3.15E+07	−3.35	0.67	E	2.84E+07	−3.39	0.46	E	8.00E+07	E
311.240	2	10	1.67E+08	−2.61	0.00	3.72E+06	−4.27	0.13	E	2.95E+08	−2.37	0.37	E	7.00E+07	E
312.240	2	9	3.14E+08	−2.34	0.00	1.52E+08	−2.65	0.19	E	4.07E+08	−2.23	0.28	E	2.90E+08	E
314.267	1	6	7.93E+05	−4.93	0.00	5.27E+07	−3.11	0.20	E	6.10E+08	−2.04	0.06	E	3.10E+08	E
314.397	3	54	6.51E+07	−3.02	0.01	1.37E+06	−4.69	0.90	E	2.77E+07	−3.39	0.68	E	7.00E+07	E
315.454	3	53	6.95E+08	−1.98	0.01	3.38E+08	−2.30	0.36	E	2.48E+08	−2.43	0.42	E	8.90E+08	E
315.882	1	5	4.46E+08	−2.18	0.00	5.74E+07	−3.07	0.46	E	2.47E+08	−2.43	0.34	E	2.60E+08	E
324.835	2	8	1.50E+08	−2.62	0.00	7.99E+07	−2.90	0.04	E	1.51E+08	−2.62	0.44	E	9.00E+07	E
324.988	2	7	5.14E+07	−3.09	0.00	1.04E+06	−4.78	0.11	E	4.78E+06	−4.12	0.80	E	2.00E+07	E
326.702	3	42	4.59E+08	−2.13	0.02	9.53E+07	−2.82	0.54	E	2.24E+08	−2.44	0.49	E	5.80E+08	E
328.702	3	40	2.82E+08	−2.34	0.07	1.26E+08	−2.69	0.28	E	1.43E+08	−2.64	0.32	E	1.20E+08	E
332.008	2	5	9.83E+07	−2.79	0.00	1.26E+05	−5.68	0.96	E	5.25E+06	−4.06	0.54	E	6.00E+07	E
335.642	3	37	1.32E+09	−1.65	0.15	5.59E+06	−4.02	0.82	E	2.62E+06	−4.35	0.85	E	1.22E+09	E
339.294	3	31	5.53E+08	−2.02	0.01	2.64E+09	−1.34	0.21	E	6.94E+08	−1.92	0.60	E	1.25E+09	E
339.624	3	30	5.51E+07	−3.02	0.00	6.85E+07	−2.93	0.36	E	7.77E+07	−2.87	0.64	E	5.60E+08	E
342.094	3	28	1.25E+09	−1.66	0.04	8.57E+08	−1.82	0.06	E	8.74E+08	−1.81	0.57	E	1.18E+09	E
342.469	3	27	5.31E+09	−1.03	0.05	3.07E+08	−2.27	0.14	E	1.51E+08	−2.57	0.52	E	6.88E+09	E
344.101	3	24	1.18E+09	−1.68	0.07	1.15E+10	−0.69	0.24	E	1.49E+07	−3.58	0.72	E	3.10E+08	E
345.480	3	22	5.52E+08	−2.01	0.01	4.83E+08	−2.06	0.03	E	2.28E+09	−1.39	0.58	E	7.20E+08	E
345.690	4	76	2.17E+08	−2.41	0.01	2.78E+09	−1.30	0.12	E	4.23E+08	−2.12	0.54	E	2.60E+08	E
346.721	3	21	5.95E+08	−1.97	0.05	8.98E+08	−1.79	0.30	E	7.98E+08	−1.84	0.33	E	8.40E+08	E
346.824	3	20	3.93E+08	−2.15	0.01	1.24E+09	−1.65	0.18	E	1.64E+08	−2.53	0.59	E	7.70E+08	E
348.909	4	74	1.32E+08	−2.62	0.01	1.44E+08	−2.58	0.55	E	1.29E+07	−3.63	0.32	E	7.00E+07	E
349.072	3	16	1.21E+08	−2.66	0.01	1.01E+08	−2.73	0.37	E	1.24E+08	−2.65	0.58	E	1.20E+08	E
351.851	3	14	7.41E+08	−1.86	0.09	1.05E+08	−2.71	0.57	E	2.63E+06	−4.31	0.79	E	4.10E+08	E
352.884	3	13	4.15E+08	−2.11	0.01	2.37E+09	−1.35	0.10	E	4.74E+08	−2.05	0.63	E	9.70E+08	E
354.221	3	12	3.80E+08	−2.15	0.05	4.06E+08	−2.12	0.11	E	2.80E+07	−3.28	0.94	E	8.00E+07	E

[a] Experimental values from Ryabtsev et al. [5].
[b] Lower and upper level indices, respectively i and k, given in the first column of Table 2.
[c] Our HFR calculation.
[d] Our MCDHF-RCI-A calculation.
[e] Our MCDHF-RCI-B calculation.
[f] Hartree–Fock calculation of Ryabtsev et al. [5].
[g] Cancellation factor as defined in Cowan [7].
[h] Uncertainty indicator as defined by NIST [10], here AAA ≤ 0.3%, AA ≤ 1%, A+ ≤ 2%, A ≤ 3%, B+ ≤ 7%, B ≤ 10%, C+ ≤ 18%, C ≤ 25%, D+ ≤ 40%, D ≤ 50%, E > 50%, evaluated with respect to our HFR gA-values using the methodology described by Kramida [11].
[i] Given in the Babushkin gauge.
[j] Uncertainty indicator as defined in Ekman et al. [9].
[k] Doubly classified in Ryabtsev et al. [5].

one clearly sees that larger discrepancies of up to several orders of magnitude appear for the weak transitions with $S_{RYA} < 3$ a.u. where the ratios $gA_{RYA}/gA_{HFR} \leq 0.5$ or $gA_{RYA}/gA_{HFR} \geq 1.5$. Most of the discords are due to strong cancellation effects affecting the calculation of the line strengths of transitions characterized by $CF < 0.05$ (see Table 3). Regarding the 12 strongest transitions with $S_{RYA} \geq 3$ a.u., they all have gA_{RYA}/gA_{HFR} ratios either less than 1.5 or greater than 0.5 with an average of 1.02 and a standard deviation of 0.04. Fig. 5 presents a larger scatter of the ratios between our MCDHF-RCI-A weighted transition probabilities and our HFR values, namely gA_{RCI-A}/gA_{HFR}, with only the two strongest transitions (with $S_{RCI-A} \geq 10$ a.u.) having either $gA_{RCI-A}/gA_{HFR} > 0.5$ or $gA_{RCI-A}/gA_{HFR} < 1.5$. The situation has somewhat improved in Fig. 6. Here, there are now 7 strongest lines (with $S_{RCI-B} \geq 5$ a.u.) characterized by ratios of our MCDHF-RCI-B gA-value to our HFR value, gA_{RCI-B}/gA_{HFR} having either $gA_{RCI-B}/gA_{HFR} > 0.5$ or $gA_{RCI-B}/gA_{HFR} < 1.5$. In addition, the average ratio for these transitions is 0.86 and the corresponding standard deviation amounts to 0.12.

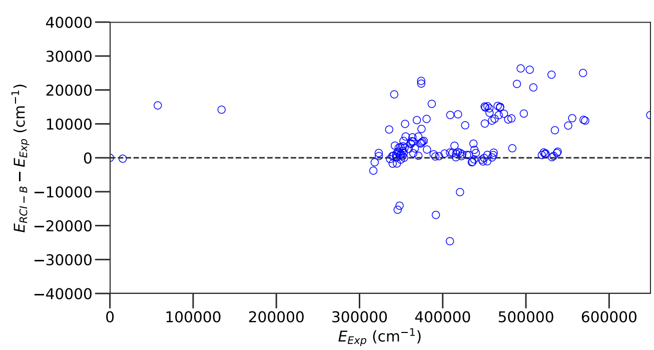

Fig. 3. Comparison of MCDHF-RCI-B energy levels with respect to experiment [5]. The energy difference is plotted versus the experimental energy. The root mean square of the differences is equal to 9580 cm^{-1}. Black dashed line: straight line of equality.

4. Conclusions

The Einstein coefficients for the spontaneous emission process and the oscillator strengths have been computed for the 237 electric dipole transitions in Ta VII observed by Ryabtsev et al. [5] in the spectral range between 191 Å and 355 Å. A multiplatform approach has been used in order to estimate the accuracy of the calculated rates as no measurement of radiative rates is available in the literature. The former consisted in building three independent models based on both the HFR [7] and the MCDHF [6,8] methods and comparing with the HFR model published in Ryabtsev et al. [5] that was constructed for line classification purpose. The uncertainties as defined by NIST [10] have been determined using our HFR calculations as a reference following a procedure described by Kramida [11]. They range from E (>50%) for most of the transitions to AAA (≤0.3%). The latter value of $Unc.$ and the good agreement between of our HFR and Ryabtsev et al. [5] rates only reflect the internal consistency of the HFR method. This

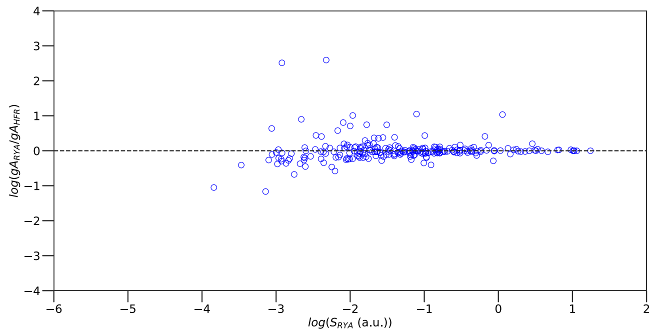

Fig. 4. Comparison of the values calculated by Ryabtsev et al. [5], gA_{RYA}, with respect to our HFR transition probabilities, gA_{HFR}. The ratio, gA_{RYA}/gA_{HFR}, is plotted versus the line strength, S_{RYA}, deduced from the A-values of Ryabtsev et al. [5] both in logarithmic scale. Black dashed line: straight line of equality. This plot is used to evaluate the uncertainty indicator as defined in NIST [10] on the Ryabtsev et al. rates following the procedure described by Kramida [11].

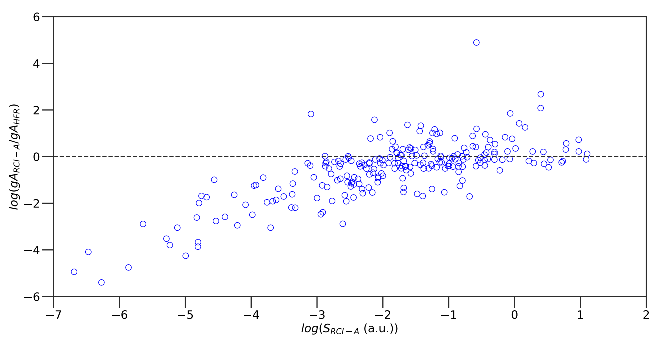

Fig. 5. Comparison of our MCDHF-RCI-A transition probabilities corrected with the experimental wavelengths [5], gA_{RCI-A}, with respect to our HFR values, gA_{HFR}. The ratio, gA_{RCI-A}/gA_{HFR}, is plotted versus our RCI-A line strength, S_{RCI-A}, both in logarithmic scale. Black dashed line: straight line of equality. This plot is used to evaluate the uncertainty indicator as defined in NIST [10] on our MCDHF-RCI-A rates following the procedure described by Kramida [11].

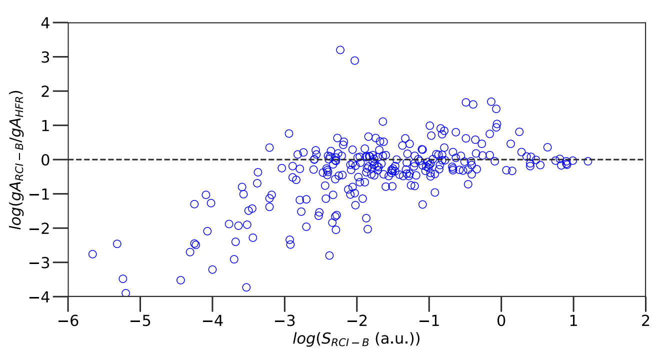

Fig. 6. Comparison of our MCDHF-RCI-B transition probabilities corrected with the experimental wavelengths [5], gA_{RCI-B}, with respect to our values, gA_{HFR}. The ratio, gA_{RCI-B}/gA_{HFR}, is plotted versus our RCI-B line strength, S_{RCI-B}, both in logarithmic scale. Black dashed line: straight line of equality. This plot is used to evaluate the uncertainty indicator as defined in NIST [10] on our MCDHF-RCI-B rates following the procedure described by Kramida [11].

is not the case for both our MCDHF models, but the strong discords with both HFR models may be due to the fact that we have neglected the correlation with the core electrons in those calculations. The latter would increase significantly the dimensions of the problem rendering the present MCDHF calculations out of reach. In conclusion, experimental A-values and/or lifetime measurements are clearly needed here. In the meantime, we recommend our HFR rates. Their uncertainties are similar to those we estimated for the results of Ryabtsev et al. [5].

CRediT authorship contribution statement

E. Bokamba Motoumba: Writing – original draft, Investigation, Formal analysis, Data curation. **S. Enzonga Yoca:** Writing – review & editing, Supervision, Funding acquisition, Conceptualization. **P. Quinet:** Writing – review & editing, Validation, Supervision, Resources, Project administration, Funding acquisition, Conceptualization. **P. Palmeri:** Writing – review & editing, Writing – original draft, Supervision, Resources, Methodology, Investigation, Funding acquisition, Formal analysis, Data curation, Conceptualization.

Declaration of competing interest

The authors declare the following financial interests/personal relationships which may be considered as potential competing interests: Patrick Palmeri reports financial support was provided by F.R.S.-FNRS. Pascal Quinet reports financial support was provided by F.R.S.-FNRS. If there are other authors, they declare that they have no known competing financial interests or personal relationships that could have appeared to influence the work reported in this paper.

Data availability

All the data are available in the paper.

Acknowledgments

PP and PQ are respectively Research Director and Research Associate of the Belgian Fund for Scientific Research F.R.S.-FNRS. Financial support from this organization is gratefully acknowledged. EBM is grateful to Belgian colleagues for their hospitality during his stay at Université de Mons – UMONS. EBM and SEY was supported by Université Marien Ngouabi from Congo.

References

[1] Linsmeier C, Rieth M, Aktaa J, Chikada T, Hoffmann A, Houden A, Kurishita H, Jin X, Li M, Litnovsky A, Matsuo S, von Müller A, Nikolic V, Palacios T, Rippan R, Qu S, Reiser J, Riesch J, Shikama T, Stieglitz R, Weber T, Wurster S, You J-H, Zhou Z. Development of advanced high heat flux and plasma-facing materials. Nucl Fusion 2017;57:092007. http://dx.doi.org/10.1088/1741-4326/aa6f71.

[2] Gilbert MR, Sublet J-C. Neutron-induced transmutation effects in W and W-alloys in a fusion environment. Nucl Fusion 2011;51:043005. http://dx.doi.org/10.1088/0029-5515/51/4/043005.

[3] Ialovega M, Dabney T, Navarro Gonzalez M, Yeom H, Velez D, Willing E, Anderson JK, Angot T, Bisson R, Forest C, Kreter A, Schmitz O, Sridharan K. Initial study on thermal stability of cold spray tantalum coating irradiated with deuterium for fusion applications. Phys Scr 2023;98:115611. http://dx.doi.org/10.1088/1402-4896/ad0098.

[4] Ryabtsev AN, Kononov EYa, Kildiyarova RR, Tchang-Brillet W-ÜL, Wyart J-F. $4f^{13}5s^25p^6 - 4f^{13}5s^25p^56s$ Transitions in the W VIII spectrum and spectra of isoelectronic hafnium, tantalum, and rhenium ions. Opt Spectrosc 2012;113:109. http://dx.doi.org/10.1134/S0030400X12080140.

[5] Ryabtsev AN, Kononov EYa, Kildiyarova RR, Tchang-Brillet W-ÜL, Wyart J-F, Champion N, Blaess C. Spectra of the W VIII isoelectronic sequence: II. Ta VII. Phys Scr 2014;89:125403. http://dx.doi.org/10.1088/0031-8949/89/12/125403.

[6] Grant IP. Relativistic quantum theory of atoms and molecules. theory and computation. New York: Springer; 2007.

[7] Cowan RD. The theory of atomic structure and spectra. Berkeley: University of California Press; 1981.

[8] Froese Fischer C, Gaigalas G, Jönsson P, Bieroń J. GRASP2018-A fortran 95 version of the general relativistic atomic structure package. Comput Phys Commun 2019;237:184. http://dx.doi.org/10.1016/j.cpc.2018.10.032.

[9] Ekman J, Godefroid M, Hartman H. Validation and implementation of uncertainty estimates of calculated transition rates. Atoms 2014;2:215. http://dx.doi.org/10.3390/atoms2020215.

[10] Kramida A, Ralchenko Yu, Reader J, NIST ASD Team. NIST atomic spectra database (ver. 5.10). Gaithersburg, MD: National Institute of Standards and Technology; 2022, http://dx.doi.org/10.18434/T4W30F, [Online]. Available: https://physics.nist.gov/asd [2023, January 18].

[11] Kramida A. Critical evaluation of data on atomic energy levels, wavelengths, and transition probabilities. Fusion Sci Technol 2013;63:313. http://dx.doi.org/10.13182/FST13-A16437.